

Maximum Margin Clustering for State Decomposition of Metastable Systems[☆]

Hao Wu*

*Department of Mathematics & Computer Science, Free University of Berlin, Arnimallee 6,
14195 Berlin, Germany*

Abstract

When studying a metastable dynamical system, a prime concern is how to decompose the phase space into a set of metastable states. Unfortunately, the metastable state decomposition based on simulation or experimental data is still a challenge. The most popular and simplest approach is geometric clustering which is developed based on the classical clustering technique. However, the prerequisites of this approach are: (1) data are obtained from simulations or experiments which are in global equilibrium and (2) the coordinate system is appropriately selected. Recently, the kinetic clustering approach based on phase space discretization and transition probability estimation has drawn much attention due to its applicability to more general cases, but the choice of discretization policy is a difficult task. In this paper, a new decomposition method designated as *maximum margin metastable clustering* is proposed, which converts the problem of metastable state decomposition to a semi-supervised learning problem so that the large margin technique can be utilized to search for the optimal decomposition without phase space discretization. Moreover, several simulation examples are given to illustrate the effectiveness of the proposed method.

Keywords: metastable states, large margin methods, clustering analysis, semi-supervised learning

1. Introduction

Metastability is an ubiquitous phenomenon which occurs in many complex systems in nature, including conformational transitions in macromolecules [2], autocatalytic chemical reactions [3] and climate changes [4]. Generally speaking, the metastability of a dynamical system means that the phase space of the system consists of multiple macrostates called *metastable states*, in which the

[☆]Some preliminary results have been reported in [1].

*Corresponding author. Tel.: +49 (0)30 838 75774.

Email address: hwu@zedat.fu-berlin.de (Hao Wu)

system tends to persist for a long time before transiting rapidly to another metastable state. In this paper, we focus on the problem of metastable state decomposition, i.e., how to partition the phase space of a given system into a set of ideal metastable states so that transitions between different metastable states are rare events, meanwhile, there is a considerable gap between the timescales of movements within and between metastable states. This is an important problem for analysis of metastable systems because:

1. Metastable state itself is often physically interesting. For instance, for biomolecules, the metastable states are related to the basins of the free energy surface, and the metastable state decomposition is helpful for seeking the native states with lowest energy and kinetic trap states with locally minimal energy which can represent the large scale geometric structures of conformations (see e.g., [5, 6]).
2. The dynamical behavior of a metastable system can be approximately described as a transition network of metastable states on a slow timescale, and such approximate description is able to provide a simple and global picture of the system dynamics which preserves the essential dynamical properties. Fig. 1 gives an example of metastable system and the its dynamical approximation. Note that the metastable state based dynamical approximation is closely related with the Markov state models (MSMs) [7], where transitions between discrete states obtained from phase space discretization are assumed to be Markovian and the corresponding transition probability matrices can be used to characterize the system dynamics. A large number of theoretical and experimental studies (see e.g., [5, 7–10]) demonstrated that a small-sized and satisfying MSM can be obtained by treating each metastable state as a Markovian state if the transition rates between different metastable states are sufficiently small compared to lifetimes of metastable states. Although the research focus of MSMs has shifted from metastability to spectral approximation and maximizing metastability has been shown to be not the optimal way to improve the accuracy of MSMs in recent years [11], the metastable state decomposition is still commonly used to construct MSMs in applications due to its ease-of-use. Moreover, it is required for some more advanced analysis and modeling techniques of metastable systems. For example, it was proved in [7, 10] that the quality of an MSM can be improved through fine discretization around boundaries between metastable states, and the hidden Markov model analysis approach of metastable systems proposed in [12] needs the metastable state decomposition for parameter initialization.

Moreover, the metastable state decomposition is also applicable to unsupervised classification problems when data are sequentially sampled and the data categories are rarely changed during sampling (e.g., classification of sensor data).

For some low-dimensional systems, metastable states can be found manually by exploring their energy landscapes (see e.g., [13–16]). But for high-dimensional and complex systems, the intuitive partitioning of the whole phase space is generally infeasible, and the metastable state decomposition can only be performed

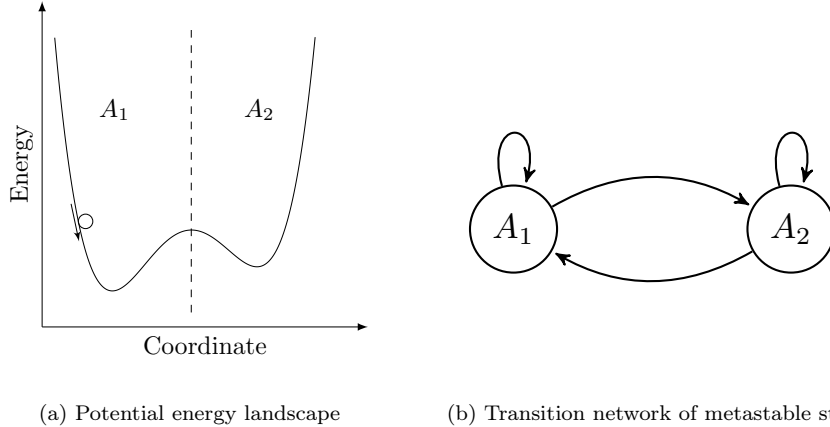


Figure 1: Illustration of dynamical approximation based on metastability decomposition. The left panel (a) shows the energy landscape of a stochastic diffusion system, which has two potential wells and can be decomposed into two metastable states A_1 and A_2 according to the energy barrier. The right panel (b) shows the corresponding transition network obtained from the metastable decomposition.

through statistical analysis of the simulation or experimental data.

The simplest approach for data based metastable state decomposition is geometric clustering, which detects the metastable states through grouping data points in phase space which are geometrically similar, and are usually implemented by classical clustering algorithms [17–21] including k -means, k -medoids, Bayesian clustering and self-organizing maps. The theory basis of this approach is that metastable states generally correspond to “energy basins” in the phase space and the local maxima of the density function of the equilibrium state distribution are then centers of metastable states. The application of the geometric clustering has two key limitations. First, it requires that the global equilibrium is reached in simulations or experiments so that the empirical distribution of the data set is consistent with the equilibrium distribution. Second, it is sensitive to the selection of the coordinates or projected coordinates of the phase space because a “bad” coordinate system may destroy the geometric structure of the energy landscape. (Note that for analysis of experimental data, the coordinate system is determined by the observation model of experiments and cannot be arbitrarily selected.) An alternative to the geometrical cluster approach is the density based clustering approach [22, 23], which tries to measure the data point density directly and cut out regions of high data point density from data sets. It is, however, rather susceptible to statistical uncertainty and noise.

A more general approach is kinetic clustering, which involves two steps: (1) discretize the phase space into small bins, and estimate the transition proba-

bilities between bins from simulation or experimental trajectories, (2) lump the discrete bins to metastable states through minimizing the transition probabilities between different metastable states. In contrast to the geometric clustering approach, this approach implements clustering based on “kinetic similarity” rather than geometric similarity, and can effectively utilize the information of the system dynamics contained in data to improve the accuracy of the decomposition. Furthermore, since the kinetic clustering method is implemented based on transition probability distributions, it only requires that simulations or experiments are in local equilibrium instead of global equilibrium [24]. From the viewpoint of Markov chain theory, the kinetic clustering for metastable state decomposition is in fact a Markov chain compression problem [8].

The most popular representatives of this approach are Perron cluster cluster analysis (PCCA) and PCCA+ [5, 25, 26], which were developed based on the principle of spectral clustering by using transition probabilities to define similarities between bins. PCCA(+) methods have been widely used in applications due to their computational efficiency and the acceptable quality, but they are only applicable to time reversible systems. In [27], a singular value decomposition based lumping algorithm for nonreversible systems was proposed. Furthermore, Jain and Stock [28] presented a “most probable path algorithm” for bin lumping in order to avoid the computation of large matrix decompositions, and a Bayesian lumping method was proposed in [29] which considers the statistical uncertainty in transition probabilities. The main difficulty of kinetic clustering comes from the choice of bins, and the boundaries of metastable states are unable to be accurately captured with a poor choice of bins. Generally speaking, the discrete bins used in kinetic clustering are still given by some geometric clustering algorithm where the system dynamics is not considered, and one can only improve the decomposition accuracy by adding more bins. But a large number of bins may cause overfitting problem in the transition probability estimation. Some recent publications [30, 31] investigated the choice of bin number from the perspective of model comparison, but how to adjust the shape of bins to meet the requirement of metastable state decomposition is still an open problem. In [32], an adaptive decomposition method was proposed, which iteratively implements the space discretization and lumping to modify boundaries of metastable states. However, the convergence of this method cannot be guaranteed.

The objective of this paper is to propose a new clustering method for metastable state decomposition based on the large margin principle. Recently, large margin techniques have received increasing attention in the machine learning community [33, 34]. For a given supervised or unsupervised classification problem, large margin techniques can improve the robustness and generalization capability of the classifier through maximizing the margin between training data and classification boundaries. In this paper, we propose an optimization model called *maximum margin metastable clustering* for metastable state decomposition by combining the large margin criterion and metastability criterion, which can effectively utilize both the geometric and the dynamical information contained in data, and develop a two-stage algorithm for searching the optimal decomposition by combining global search and local search techniques. In com-

parison with the previous decomposition approaches, this decomposition method directly constructs the boundaries of metastable states in the continuous phase space without any pre-discretization, and can achieve a reliable and robust decomposition based on the the large margin criterion even for small-scale data sets.

2. Preliminaries

In this section, we review briefly some of the relevant background on large margin learning. Given a set of training data $\{\mathbf{x}_n\}_{n=1}^N$ and their class labels $\{y_n\}_{n=1}^N$, where each \mathbf{x}_n is a data point sampled from a domain \mathcal{X} and $y_n \in \{1, \dots, \kappa\}$, the support vector machine (SVM) finds a hyperplane classifier defined by the decision rule

$$y = \operatorname{argmax}_{1 \leq k \leq \kappa} (\mathbf{w}_k^\top \phi(\mathbf{x}) + b_k) \quad (1)$$

which can map the training data to correct labels and achieve strong generalization performance through maximizing the classification margin between training data and decision boundaries. Here ϕ is a mapping function from \mathcal{X} to a feature space \mathbb{R}^d , and is generally induced by a Mercer kernel function $\operatorname{Ker}(\cdot, \cdot)$ with

$$\operatorname{Ker}(\mathbf{x}, \mathbf{x}') = \phi(\mathbf{x})^\top \phi(\mathbf{x}') \quad (2)$$

The optimal decision rule of SVM can be obtained by solving the following optimization problem [33]:

$$\begin{aligned} \min_{\mathbf{W}, \mathbf{b}} \quad & \frac{1}{2} \|\mathbf{W}\|^2 \\ \text{s.t.} \quad & \forall n = 1, \dots, N, \quad k = 1, \dots, \kappa, \\ & (\mathbf{w}_{y_n}^\top - \mathbf{w}_k^\top) \phi(\mathbf{x}_n) + (b_{y_n} - b_k) + 1_{y_n=k} \geq 1. \end{aligned} \quad (3)$$

where $\mathbf{W} = (\mathbf{w}_1^\top, \dots, \mathbf{w}_\kappa^\top)^\top$ and $\mathbf{b} = (b_1, \dots, b_\kappa)^\top$. The constraint of (3), called *large margin constraint*, states that for each training data \mathbf{x}_n , the decision function value of \mathbf{x}_n for the true class y_n exceeds the decision function value for any other competing class $k \neq y_n$ by at least one, and $\|\mathbf{W}\|$ can be shown to be inversely proportional to the classification margin in the feature space under the large margin constraint. Note that (3) is a quadratic programming and the global optimum can be efficiently found by convex optimization methods. However, in many practical cases, there is no feasible solution which satisfies the large margin constraint exactly due to the linear non-separability of training data, and we can only seek a large margin classifier which separates the data ‘‘as much as possible’’. In order to achieve this, we can introduce a slack variable ξ_n for each \mathbf{x}_n and modify the optimization problem (3) as

$$\begin{aligned} \min_{\mathbf{W}, \mathbf{b}, \xi} \quad & \frac{1}{2} \beta \|\mathbf{W}\|^2 + \frac{1}{N} \mathbf{1}^\top \xi \\ \text{s.t.} \quad & \forall n = 1, \dots, N, \quad k = 1, \dots, \kappa, \\ & (\mathbf{w}_{y_n}^\top - \mathbf{w}_k^\top) \phi(\mathbf{x}_n) + (b_{y_n} - b_k) + 1_{y_n=k} \geq 1 - \xi_n. \end{aligned} \quad (4)$$

where $\boldsymbol{\xi} = (\xi_1, \dots, \xi_N)^\top$ and $\beta > 0$ is the regularization parameter. It can be observed from constraints of (4) that $\xi_n \geq 0$ for all n , and $\xi_n > 0$ if and only if $(\mathbf{w}_{y_n}^\top \boldsymbol{\phi}(\mathbf{x}_n) + b_{y_n}) - (\mathbf{w}_k^\top \boldsymbol{\phi}(\mathbf{x}_n) + b_k) \geq 1$ does not hold for some $k \neq n$. Therefore we can conclude that ξ_n represents the misclassification loss of \mathbf{x}_n , and the objective function of (4) balances the empirical risk on the training data versus the classification margin.

Remark 1. It is worth pointing out that SVM was originally designed for two-class classification [35]. A variety of strategies have been proposed to extend the SVM for multi-class problems, such as one-against-all [36], one-against-one [37] and error-correcting output coding [38]. Here we select the multi-class SVM proposed in [33] which minimizes the the multi-class margin loss directly, because it is more “logical” than the other strategies from the perspective of large margin learning and can be easily applied to unsupervised learning problems (see below).

Maximum margin clustering (MMC) [39, 40] extends the maximum margin principle to unsupervised learning, i.e., data clustering. For a set of unlabeled data $\{\mathbf{x}_n\}$, MMC targets to construct a maximum margin decision rule by optimizing (4) with both (\mathbf{W}, \mathbf{b}) and data labels $\{y_n\}$ being decision variables. But in this unsupervised case, the optimization problem (4) has a trivially optimal solution with $y_n \equiv 1$ and $\|\mathbf{W}\| = 0$, which implies that all data are assigned to the same class and an infinite classification margin is obtained. To prevent such physically meaningless solutions with empty classes, the following class balance constraint is required for MMC:

$$\varrho_l N \leq \sum_{m=1}^N 1_{y_m=k} \leq \varrho_u N, \quad \forall k = 1, \dots, \kappa \quad (5)$$

where ϱ_l, ϱ_u denote the lower and upper bounds of the proportion of each class size, and satisfy $0 < \varrho_l < 1/\kappa < \varrho_u < 1$. Then, the complete MMC problem (with slack variables) can be formulated as

$$\begin{aligned} \min_{\mathbf{y}, \mathbf{W}, \mathbf{b}, \boldsymbol{\xi}} \quad & \frac{1}{2} \beta \|\mathbf{W}\|^2 + \frac{1}{N} \mathbf{1}^\top \boldsymbol{\xi} \\ \text{s.t.} \quad & \forall n = 1, \dots, N, \quad k = 1, \dots, \kappa, \\ & (\mathbf{w}_{y_n}^\top - \mathbf{w}_k^\top) \boldsymbol{\phi}(\mathbf{x}_n) + (b_{y_n} - b_k) + 1_{y_n=k} \geq 1 - \xi_n, \\ & \varrho_l N \leq \sum_{m=1}^N 1_{y_m=k} \leq \varrho_u N. \end{aligned} \quad (6)$$

with $\mathbf{y} = (y_1, \dots, y_N) \in \{1, \dots, \kappa\}^N$. In contrast with the SVM problem (4), (6) is a nonconvex mixed-integer problem and much more difficult to solve. The existing optimization methods for the MMC problem can be roughly categorized into two types. The first type of method relaxes the MMC problem into a semidefinite programming (SDP) problem that can be globally optimized by standard SDP solvers [40, 41]. However, this type of method is very computationally expensive and can only be applied to small data sets. The other type of method utilizes some local search algorithms, such as concave-convex procedure [42] and alternating optimization [43], to solve the MMC problem directly, which

is more efficient than the relaxation method but usually suffers from undesired local minima.

Remark 2. The balance constraint (5) is also useful to avoid the problem of separating a single outlier (or very small group of outliers) from the rest of the data, and allows one to incorporate the prior knowledge on the balance of data distribution. The theoretical analysis and empirical research on the balance constraint is still very limited and the parameters ϱ_l, ϱ_u are usually selected by trial and error. According to our numerical experience, the parameters can be simply set as $[\varrho_l, \varrho_u] = [\epsilon, 1 - \epsilon]$ with $\epsilon = 10^{-3} \sim 10^{-1}$, and the value of ϵ influences only a little on clustering results. Moreover, it is worth pointing out that the balance constraints $[\varrho_l, \varrho_u] = [0, 1]$ and $[\varrho_l, \varrho_u] = [\epsilon, 1 - \epsilon]$ with ϵ being positive and sufficiently small are completely different in essence for MMC. The former one is always an “inactive” constraint and the optimal decision boundary is infinitely far away from all the data, and the latter one enforces that the optimal decision boundary of MMC must pass through the data set.

Remark 3. For some commonly used Mercer kernel functions (e.g., Gaussian kernels), the dimensions of the corresponding feature spaces are extremely high or infinite, and the direct feature mappings are impossible. In such a case, the kernel trick can be used to solve the SVM or MMC problem by performing the feature mapping implicitly based on the kernel matrix $\mathbf{K} = [K_{ij}] = [\text{Ker}(\mathbf{x}_i, \mathbf{x}_j)] \in \mathbb{R}^{N \times N}$ (see [33, 40] for details). While the kernel trick has been widely and successfully applied in large margin learning, the calculation of kernel matrices is a bottleneck of the kernel trick for large-scale data sets. In recent years, a lot of alternatives to the kernel trick have been proposed to reduce the computational and storage costs (see, e.g., [43–46]), which can approximate the induced feature mapping ϕ by a low dimensional function $\hat{\phi}(\mathbf{x})$ such that

$$\phi(\mathbf{x})^\top \phi(\mathbf{x}') = \text{Ker}(\mathbf{x}, \mathbf{x}') \approx \hat{\phi}(\mathbf{x})^\top \hat{\phi}(\mathbf{x}'), \quad \forall \mathbf{x}, \mathbf{x}' \in \mathcal{X} \quad (7)$$

Therefore, in this paper, we only consider the case that the feature mapping ϕ can be explicitly defined and computed.

3. Maximum margin metastable clustering

In this section, we apply the framework of large margin learning to metastability analysis. Suppose that we have L trajectories $\{\mathbf{x}_1^1, \dots, \mathbf{x}_{M_1}^1\}, \{\mathbf{x}_1^2, \dots, \mathbf{x}_{M_2}^2\}, \dots, \{\mathbf{x}_1^L, \dots, \mathbf{x}_{M_L}^L\}$ in a phase space \mathcal{X} which are generated by simulations or experiments of a dynamical system, where the point \mathbf{x}_t^l represents the system state at time t in the l -th run, and M_l denotes the time length of the l -th run. Furthermore, for convenience of notation, we define

$$\mathcal{P} = \{(\bar{\mathbf{x}}_n, \mathbf{x}_n)\}_{n=1}^N = \{(\mathbf{x}_t^l, \mathbf{x}_{t+1}^l) | 1 \leq l \leq L, 1 \leq t < M_l\} \quad (8)$$

as the set of all transition pairs that appear in trajectories. The purpose of metastable state decomposition is to partition \mathcal{X} into κ subspaces (*metastable*

states), so that it is a rare event – not only for the given L trajectories but also for new trajectories generated by the same system – that \mathbf{x}_t and \mathbf{x}_{t+1} belong to different metastable states.

Remark 4. An important issue for metastable state decomposition is determining the value of κ . But this issue is beyond the scope of this paper and we simply assume that κ is given. In practical applications, κ can be obtained by analyzing of life times of metastable states (see [5] for details).

Analogous to learning in SVM and MMC, we can construct a large margin decision rule for metastable state decomposition based on the following criteria:

1. **Metastability criterion.** For most of state transition pairs $(\bar{\mathbf{x}}_n, \mathbf{x}_n) \in \mathcal{P}$, $\bar{\mathbf{x}}_n$ and \mathbf{x}_n should be classified to the same metastable state, which implies that the boundaries between metastable states are rarely crossed in runs of the system.
2. **Large margin criterion.** The metastable state boundaries should be placed as far away from the trajectory data as possible in order to improve the generalization performance of the decomposition result for unknown trajectories.

The two criteria leads to a maximum margin metastable clustering (M³C) method that minimizes $\|\mathbf{W}\|$ under the following *large margin metastable constraint*:

$$\begin{aligned} (\mathbf{w}_{y_n}^\top - \mathbf{w}_k^\top) \phi(\bar{\mathbf{x}}_n) + (b_{y_n} - b_k) + 1_{y_n=k} &\geq 1 \\ (\mathbf{w}_{y_n}^\top - \mathbf{w}_k^\top) \phi(\mathbf{x}_n) + (b_{y_n} - b_k) + 1_{y_n=k} &\geq 1, \quad \forall n, k \end{aligned} \quad (9)$$

where $y_n \in \{1, \dots, \kappa\}$ denotes the metastable state label of $\bar{\mathbf{x}}_n$ and \mathbf{x}_n . It can be seen that M³C is in fact a semi-supervised learning method which can be interpreted as follows:

1. The constraint enforces $\bar{\mathbf{x}}_n$ and \mathbf{x}_n being assigned to the same metastable state for each state transition pair $(\bar{\mathbf{x}}_n, \mathbf{x}_n)$.
2. For any $\mathbf{x} \in \bigcup_{n=1}^N \{\bar{\mathbf{x}}_n, \mathbf{x}_n\}$, if it is assigned to the metastable state y , the the distances between \mathbf{x} and the boundaries of y are

$$\frac{(\mathbf{w}_y^\top - \mathbf{w}_k^\top) \phi(\mathbf{x}) + (b_y - b_k)}{\|\mathbf{w}_y - \mathbf{w}_k\|} \geq \frac{1}{\|\mathbf{w}_y - \mathbf{w}_k\|}, \quad \text{for } k \neq y \quad (10)$$

Then the margin between data and decision boundaries can be increased by minimizing the objective function $\|\mathbf{W}\|$ of M³C.

Moreover, it is interesting to note that the M³C method can be expressed as a specific MMC method in the space of transition pairs $(\bar{\mathbf{x}}_n, \mathbf{x}_n)$, which seeks a decision rule

$$(\bar{y}, y) = \underset{\bar{k}, k}{\operatorname{argmax}} \mathbf{w}_{\bar{k}k}^\top \phi(\bar{\mathbf{x}}, \mathbf{x}) + b_{\bar{k}k} \quad (11)$$

under a large margin constraint

$$\left(\mathbf{w}_{y_n y_n}^\top - \mathbf{w}_{\bar{k}k}^\top \right) \phi(\bar{\mathbf{x}}_n, \mathbf{x}_n) + \left(b_{y_n y_n} - b_{\bar{k}k} \right) + 1_{y_n = \bar{k} = k} \geq 1 \quad (12)$$

where $\mathbf{w}_{\bar{k}k} = (\mathbf{w}_{\bar{k}}^\top, w_k^\top)^\top$, $b_{\bar{k}k} = b_{\bar{k}} + b_k$ and $\phi(\bar{\mathbf{x}}_n, \mathbf{x}_n) = (\phi(\bar{\mathbf{x}}_n)^\top, \phi(\mathbf{x}_n)^\top)^\top$ denotes the extended feature function. (The proof of the equivalence between (9) and (12) is given in Appendix 30.) The decision rule (11) can map a transition pair in the phase space to a pair of metastable state labels, and the constraint (12) restricts that all transition pairs in \mathcal{P} are not only far away from the decision boundaries in the product feature space $\phi(\mathcal{X}) \times \phi(\mathcal{X})$ but also enclosed in the area $\cup_{k=1}^{\kappa} \{(\bar{\mathbf{x}}, \mathbf{x}) | (k, k) = \operatorname{argmax}_{\bar{k}, k} w_{\bar{k}k}^\top \phi(\bar{\mathbf{x}}, \mathbf{x}) + b_{\bar{k}k}\}$.

Based on the above discussion, as well as by introducing slack variables and the class balance constraint as in MMC, we can formulate the M³C problem as

$$\begin{aligned}
 \min_{\mathbf{y}, \mathbf{W}, \mathbf{b}, \xi} \quad & \frac{1}{2} \beta \|\mathbf{W}\|^2 + \frac{1}{N} \mathbf{1}^\top \xi \\
 \text{s.t.} \quad & \forall n = 1, \dots, N, \quad \forall \bar{k}, k = 1, \dots, \kappa, \\
 & \left(\mathbf{w}_{y_n y_n}^\top - \mathbf{w}_{\bar{k}k}^\top \right) \phi(\bar{\mathbf{x}}_n, \mathbf{x}_n) \\
 & + \left(b_{y_n y_n} - b_{\bar{k}k} \right) + 1_{y_n = \bar{k} = k} \geq 1 - \xi_n, \\
 & \varrho_l N \leq \sum_{m=1}^N 1_{y_m = \bar{k}} \leq \varrho_u N.
 \end{aligned} \tag{13}$$

4. Comparison of maximum margin metastable clustering with relative methods

Fig. 2 shows a two dimensional and two-class example to illustrate the difference between the ideas of MMC and M³C (or the other geometric clustering methods). In this example, all the trajectory data are distributed in areas A_1 , A_2 and A_3 , and A_1 is far away from A_2 and A_3 . As shown in Fig. 2a, the optimal decision boundary founded by MMC is a horizontal line for which can achieve the maximum classification margin, and then MMC decomposes the three areas as $\{A_1\} \cup \{A_2, A_3\}$. Fig. 2b displays both data points and trajectories. As can be seen, the MMC decomposition severely violates the large margin metastable constraint because of the existence of frequent switches between A_1 and A_2 in trajectories, and the optimal decomposition provided by M³C (with an appropriate class balance constraint) is then $\{A_1, A_2\} \cup \{A_3\}$. Obviously, the decomposition result of M³C is more reasonable from the view of metastability analysis. From this example we can observe that the M³C method is able to exploit the information on both phase space distribution and metastable dynamics contained in the trajectory data by using the large margin metastable constraint.

Compared with the kinetic clustering methods of metastable state decomposition (e.g., PCCA+), the M³C method directly minimizes the ‘‘loss’’ caused by boundary crossings between metastable states without an explicit model of the system dynamics. Therefore, plenty of statistical problems which are essential and difficult for kinetic clustering methods, including the choice of space discretization and the estimation of transition probabilities, are not present in M³C. Furthermore, the large margin criterion used in M³C provides a convenient and powerful way to reduce the influence of statistical noise. Although some kinetic clustering methods can also handle the statistical noise in a Bayesian

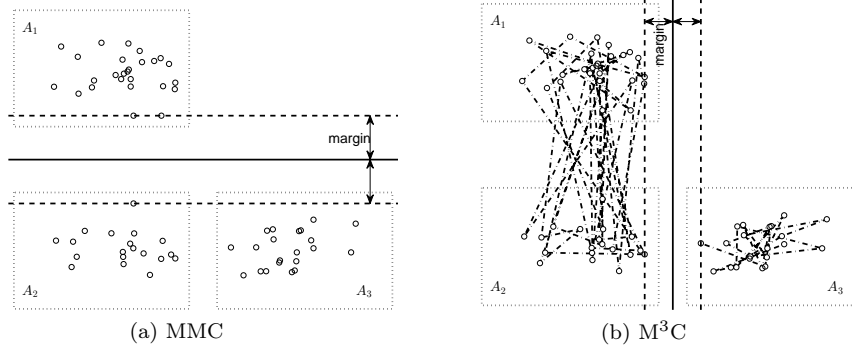


Figure 2: Illustration of decision boundaries obtained by MMC and M³C, where solid lines are decision boundaries, dashed lines show the margins, dash-dot lines represent phase space trajectories, and circles denote data points sampled from the trajectories.

manner (see e.g., [29]), M³C offers the advantage of naturally achieving good performance of generalization and robustness without assuming any prior distribution.

The major challenge of M³C arises from (13), which is a nonconvex mixed-integer optimization problem as the MMC problem (6). Due to the similarity between the MMC and M³C problems, solving of the latter encounters similar difficulties: the SDP relaxation based global search requires a high computational cost and the local search easily gets stuck in poor local optima.

5. Optimization method for metastable maximum margin clustering

In this section, we will propose a coarse graining based strategy to solve the M³C problem (13) that takes advantages of both global search and local search methods, and is applicable to large-scale data sets. The proposed optimization procedure can be sketched in the following steps:

1. **Coarse graining.** Discretize the space $\mathcal{X} \times \mathcal{X}$ of transition pairs into N^c ($\kappa < N^c \ll N$) bins and approximate \mathcal{P} by a coarse-grained data set $\mathcal{P}^c = \{(\bar{\mathbf{x}}_n^c, \mathbf{x}_n^c)\}_{n=1}^{N^c}$ with normalized weights $\{c_n\}$, where $(\bar{\mathbf{x}}_n^c, \mathbf{x}_n^c)$ denotes the center of the n -th bin and c_n is proportional to the number of transition pairs contained in the n -th bin. This step can be done by k -means, k -medoids or any other traditional clustering algorithm, and the value of N^c is chosen based on the limitation of computational resources.
2. **Global search.** Perform M³C on the coarse-grained data set \mathcal{P}^c by using the SDP relaxation method. Note that \mathcal{P}^c only has a small number of distinct elements, then a satisfactory solution can be achieved in this step without too much computing burden.

3. **Local search.** Refine the solution obtained in the global search step by applying some local search algorithm to the M³C problem on \mathcal{P} . Here we select the alternating optimization presented in [43] to perform the local search because it is computationally efficient and can handle the class balance constraint easily.

Below we will discuss the last two steps in more detail.

5.1. Global search

For convenience of analysis and computation, we confine that all decision hyperplanes pass through the origin in the feature space, i.e., $b_1 = \dots = b_\kappa = 0$. (This is a mild restriction especially for high dimensional feature spaces, since it reduces the number of freedom degrees of decision hyperplanes only by one.) Then the M³C problem on \mathcal{P}^c can be expressed as

$$\begin{aligned} \min_{\mathbf{y}^c, \mathbf{W}, \boldsymbol{\xi}^c} \quad & \frac{1}{2}\beta \|\mathbf{W}\|^2 + \mathbf{c}^\top \boldsymbol{\xi}^c \\ \text{s.t.} \quad & \forall n = 1, \dots, N^c, \quad \forall \bar{k}, k = 1, \dots, \kappa, \\ & \left(\mathbf{w}_{y_n^c}^\top - \mathbf{w}_{\bar{k}k}^\top \right) \phi(\bar{\mathbf{x}}_n^c, \mathbf{x}_n^c) + 1_{y_n^c = \bar{k} = k} \geq 1 - \xi_n^c, \\ & \varrho_l \leq \sum_{m=1}^{N^c} 1_{y_m^c = \bar{k}} \cdot c_m \leq \varrho_u. \end{aligned} \quad (14)$$

where $y_n^c \in \{1, \dots, \kappa\}$ and ξ_n^c denotes the label and slack variable of the n -th coarse-grained transition pair $(\bar{\mathbf{x}}_n^c, \mathbf{x}_n^c)$, $\mathbf{y}^c = (y_1^c, \dots, y_{N^c}^c)$, $\boldsymbol{\xi}^c = (\xi_1^c, \dots, \xi_{N^c}^c)^\top$, and $\mathbf{c} = (c_1, \dots, c_{N^c})^\top$ denotes the vector of weights of coarse-grained transition pairs. It is clear that the assignment \mathbf{y}^c in (14) can be represented by the equivalence relation matrices $\mathbf{D} \in \mathbb{R}^{N^c \times \kappa}$ and $\mathbf{M} \in \mathbb{R}^{N^c \times N^c}$ which are defined by

$$\mathbf{D} = [D_{ij}] = [1_{y_i^c = j}], \quad \mathbf{M} = [M_{ij}] = [1_{y_i^c = y_j^c}] \quad (15)$$

i.e., the (i, j) -th element of \mathbf{D} indicates if the label of $(\bar{\mathbf{x}}_i^c, \mathbf{x}_i^c)$ is j , and the (i, j) -th element of \mathbf{M} indicates if $(\bar{\mathbf{x}}_i^c, \mathbf{x}_i^c)$ and $(\bar{\mathbf{x}}_j^c, \mathbf{x}_j^c)$ are assigned to the same label.

Replacing \mathbf{y}^c by (\mathbf{M}, \mathbf{D}) as assignment variables in (14) and using the strong duality theorem, we can get an equivalent form of the coarse-grained M³C problem.

Theorem 5. *Solving (14) is equivalent to solving the optimization problem*

$$\begin{aligned} \min_{\mathbf{M}, \mathbf{D}, \boldsymbol{\alpha}, \boldsymbol{\theta}} \quad & \frac{1}{2}\boldsymbol{\theta}^\top \boldsymbol{\theta} - \mathbf{c}^\top \boldsymbol{\alpha} - \frac{1}{2\beta} \text{tr}(\mathbf{MCK}^s \mathbf{C}) + \mathbf{1}^\top \mathbf{c} \\ \text{s.t.} \quad & \mathbf{q}(\mathbf{D}) + (\mathbf{1} \otimes \mathbf{I}) \boldsymbol{\alpha} + \mathbf{R}\boldsymbol{\theta} \leq 0, \\ & \varrho_l \leq \mathbf{M}\mathbf{c} \leq \varrho_u, \\ & \text{diag}(\mathbf{M}) = \mathbf{1}, \\ & \mathbf{M} = \mathbf{D}\mathbf{D}^\top, \\ & \mathbf{M} \in \{0, 1\}^{N^c \times N^c}, \mathbf{D} \in \{0, 1\}^{N^c \times \kappa}. \end{aligned} \quad (16)$$

where \mathbf{C} is a diagonal matrix with the elements of \mathbf{c} on the diagonal, $\mathbf{q}(\mathbf{D})$ is a linear function of \mathbf{D} defined in (B.10), and definitions of \mathbf{K}^s and \mathbf{R} are given by (B.6) and (B.12).

Proof. See Appendix B. \square

Remark 6. The last four constraints on \mathbf{M} and \mathbf{D} of (16) come from the fact that *there is a \mathbf{y}^c such that (15) holds if and only if \mathbf{M} and \mathbf{D} are both binary matrices and satisfy $\text{diag}(\mathbf{M}) = \mathbf{1}$ and $\mathbf{M} = \mathbf{D}\mathbf{D}^\top$* [34].

It is easy to see that (16) is a convex optimization problem if we drop the constraints that \mathbf{M} and \mathbf{D} are binary matrices and the nonlinear constraint $\mathbf{M} = \mathbf{D}\mathbf{D}^\top$. This motivates an approximation method for solving the coarse-grained M³C problem based on two relaxations as in [34]. The first relaxation allows elements of \mathbf{M} and \mathbf{D} to take values in $[0, 1]$ instead of $\{0, 1\}$ and the second relaxation is to replace $\mathbf{M} = \mathbf{D}\mathbf{D}^\top$ with a convex inequality $\mathbf{M} \succeq \mathbf{D}\mathbf{D}^\top$. By using these two relaxations, (16) can be relaxed to a convex optimization problem:

$$\begin{aligned} \min_{\mathbf{M}, \mathbf{D}, \boldsymbol{\alpha}, \boldsymbol{\theta}} \quad & \frac{1}{2} \boldsymbol{\theta}^\top \boldsymbol{\theta} - \mathbf{c}^\top \boldsymbol{\alpha} - \frac{1}{2\beta} \text{tr}(\mathbf{M}\mathbf{C}\mathbf{K}^s \mathbf{C}) + \mathbf{1}^\top \mathbf{c} \\ \text{s.t.} \quad & \mathbf{q}(\mathbf{D}) + (\mathbf{1} \otimes \mathbf{I}) \boldsymbol{\alpha} + \mathbf{R}\boldsymbol{\theta} \leq 0, \\ & \varrho_l \leq \mathbf{M}\mathbf{c} \leq \varrho_u, \\ & \text{diag}(\mathbf{M}) = \mathbf{1}, \\ & \mathbf{M} \succeq \mathbf{D}\mathbf{D}^\top, \\ & 0 \leq \mathbf{M} \leq \mathbf{1}, 0 \leq \mathbf{D} \leq \mathbf{1}. \end{aligned} \tag{17}$$

According to the Schur complement lemma [47], we can further reformulate (17) in a more convenient form:

$$\begin{aligned} \min_{\mathbf{M}, \mathbf{D}, \boldsymbol{\alpha}, \boldsymbol{\theta}, \zeta} \quad & \zeta \\ \text{s.t.} \quad & \begin{bmatrix} \mathbf{I} & \boldsymbol{\theta} \\ \boldsymbol{\theta}^\top & 2\left(\zeta + \mathbf{c}^\top \boldsymbol{\alpha} + \frac{1}{2\beta} \text{tr}(\mathbf{M}\mathbf{C}\mathbf{K}^s \mathbf{C}) - \mathbf{1}^\top \mathbf{c}\right) \end{bmatrix} \succeq 0, \\ & \mathbf{q}(\mathbf{D}) + (\mathbf{1} \otimes \mathbf{I}) \boldsymbol{\alpha} + \mathbf{R}\boldsymbol{\theta} \leq 0, \\ & \varrho_l \leq \mathbf{M}\mathbf{c} \leq \varrho_u, \\ & \text{diag}(\mathbf{M}) = \mathbf{1}, \\ & \begin{bmatrix} \mathbf{I} & \mathbf{D}^\top \\ \mathbf{D} & \mathbf{M} \end{bmatrix} \succeq 0, \\ & 0 \leq \mathbf{M} \leq \mathbf{1}, 0 \leq \mathbf{D} \leq \mathbf{1}. \end{aligned} \tag{18}$$

It is an SDP problem and can be solved in polynomial time.

Since the optimal \mathbf{M} obtained from (18) is a symmetric matrix satisfying $\text{diag}(\mathbf{M}) = \mathbf{1}$ and $0 \leq \mathbf{M} \leq \mathbf{1}$, it can be interpreted as a similarity matrix of \mathcal{P}^c with each element M_{ij} representing some measure of the similarity between $(\bar{\mathbf{x}}_i^c, \mathbf{x}_i^c)$ and $(\bar{\mathbf{x}}_j^c, \mathbf{x}_j^c)$. Hence, we can utilize the spectral clustering method to recover \mathbf{y}^c from the optimal \mathbf{M} such that $M_{ij} = 1_{y_i^c = y_j^c}$ approximately holds for all i, j .

Remark 7. Obviously, the relaxation method proposed in this section can be directly applied to the original M³C problem (13) without any coarse graining, and the corresponding relaxed problem can be solved even in the case that we do not know the feature mapping implicitly but only know the kernel function

$\text{Ker}(\cdot, \cdot)$. However, this scheme is generally computationally infeasible because the it involves an SDP problem with $O(N^2)$ parameters.

5.2. Local search

We now investigate how to refine the clustering result obtained in the global search by local search. A natural way to do this is to alternatively minimize (13) with respect to (\mathbf{W}, \mathbf{b}) keeping \mathbf{y} fixed and vice versa until convergence, where the initial value of \mathbf{y} is given by the coarse-grained label assignment \mathbf{y}^c with

$$y_n = y_i^c, \text{ if } (\bar{\mathbf{x}}_n, \mathbf{x}_n) \text{ is in the bin centered at } (\bar{\mathbf{x}}_i^c, \mathbf{x}_i^c) \quad (19)$$

Note that the M³C problem (13) with a fixed \mathbf{y} is just a standard quadratic programming problem. Here we only discuss the optimization problem with respect to \mathbf{y} . For fixed \mathbf{W} and \mathbf{b} , (13) is reduced to

$$\begin{aligned} \min_{\mathbf{y}} \quad & \mathbf{1}^\top \boldsymbol{\xi} \\ \text{s.t.} \quad & \forall n = 1, \dots, N, \quad \forall \bar{k}, k = 1, \dots, \kappa, \\ & \left(\mathbf{w}_{y_n y_n}^\top - \mathbf{w}_{\bar{k}k}^\top \right) \phi(\bar{\mathbf{x}}_n, \mathbf{x}_n) \\ & + \left(b_{y_n y_n} - b_{\bar{k}k} \right) + 1_{y_n = \bar{k} = k} \geq 1 - \xi_n, \\ & \varrho_l N \leq \sum_{m=1}^N 1_{y_m = \bar{k}} \leq \varrho_u N. \end{aligned} \quad (20)$$

It is simple to verify that (20) can be transformed into a binary linear programming problem

$$\begin{aligned} \min_{\mathbf{D}^f} \quad & \text{tr}(\mathbf{H}^\top \mathbf{D}^f) \\ \text{s.t.} \quad & \varrho_l N \leq \mathbf{1}^\top \mathbf{D}^f \leq \varrho_u N, \\ & \mathbf{D}^f \in \{0, 1\}^{N \times \kappa}. \end{aligned} \quad (21)$$

where $\mathbf{D}^f = [D_{ij}^f]$ is a relation matrix with $D_{ij}^f = 1_{y_i=j}$, and $\mathbf{H} = [H_{ij}]$ is defined by

$$H_{ij} = \max_{\bar{k}, k} 1 - 1_{j=\bar{k}=k} - \left(\mathbf{w}_{jj}^\top - \mathbf{w}_{\bar{k}k}^\top \right) \phi(\bar{\mathbf{x}}_i, \mathbf{x}_i) - \left(b_{jj} - b_{\bar{k}k} \right) \quad (22)$$

Although (21) belongs to the class of NP-hard problems, it can be efficiently tackled by enumeration and cutting-plane techniques [48] in practice, and there exist a lot of software packages for solving large-scale integer programming problems like (21), including MOSEK [49], Gurobi [50] and GLPK [51].

Remark 8. It was reported in [43] that the alternating optimization method for MMC often suffers from premature convergence and can only change a small proportion of data labels even with a poor initialization, but our numerical experiments show that this problem is not serious for the local search procedure of M³C. The analysis of this phenomenon requires further investigation and we only give a rough explanation here. Generally speaking, the switching between metastable states can be observed many times in trajectories. Therefore, during the local search of M³C, there are always a number of transition pairs that

Algorithm 1 Optimization procedure for M³C

-
- 1: generate a coarse-grained transition pair set \mathcal{P}^c with cardinality N^c and normalized weights $\mathbf{c} = (c_1, \dots, c_{N^c})^\top$ from \mathcal{P} by the k -means or k -medoids algorithm
 - 2: find $(\mathbf{M}^*, \mathbf{D}^*)$ as the solution to the SDP problem (18)
 - 3: perform the spectral clustering algorithm with similarity matrix \mathbf{M}^* to get class labels $\mathbf{y}^c = (y_1^c, \dots, y_{N^c}^c)$ of coarse-grained transition pairs in \mathcal{P}^c
 - 4: calculate class labels $\mathbf{y} = (y_1, \dots, y_N)$ of transition pairs in \mathcal{P} from \mathbf{y}^c by (19)
 - 5: initialize with $\mathbf{y}^{(0)} = \mathbf{y}$ and $r = 1$
 - 6: **repeat**
 - 7: find $(\mathbf{W}^*, \mathbf{b}^*)$ as the solution to the quadratic programming problem (13) with \mathbf{y} fixed to be $\mathbf{y}^{(r-1)}$ and set $(\mathbf{W}^{(r)}, \mathbf{b}^{(r)}) = (\mathbf{W}^*, \mathbf{b}^*)$
 - 8: find $\mathbf{D}^{f*} = [D_{ij}^{f*}]$ as the solution to the binary linear programming problem (21) with (\mathbf{W}, \mathbf{b}) set to be $(\mathbf{W}^{(r)}, \mathbf{b}^{(r)})$.
 - 9: calculate $\mathbf{y}^* = (y_1^*, \dots, y_N^*)$ by $y_n^* = \operatorname{argmax}_j D_{nj}^{f*}$ and set $\mathbf{y}^{(r)} = \mathbf{y}^*$
 - 10: set $r := r + 1$
 - 11: **until** the Hamming distance between $\mathbf{y}^{(r)}$ and $\mathbf{y}^{(r-1)}$ is less than or equal to a given constant α_H or r is larger than a pre-defined threshold r_{\max}
 - 12: **return** $(\mathbf{W}^{(r)}, \mathbf{b}^{(r)}, \mathbf{y}^{(r)})$
-

are close to the decision boundaries and violate the large margin metastable constraint with not-so-small slack values even if $\beta \ll 1$. These misclassified transition pairs are helpful to “push” the decision boundaries away from the initial positions and their labels can be easily changed especially in early iterations of the local search.

5.3. Full description of the optimization procedure

Based on the above analysis, the complete optimization method developed for M³C can be summarized in Algorithm 1.

6. Experiments

In this section, we demonstrate the performance of the proposed decomposition method on some synthetic metastable systems and molecular dynamics simulations.

The detailed settings of Algorithm 1 for M³C are as follows:

- In the coarse graining step, \mathcal{P}^c is provided by the standard k -medoids algorithm [52] with $N^c = 30$. (Here we use k -medoids rather than k -means because k -medoids is more robust to outliers and can avoid the appearance of the coarse-grained transitions which make no physical sense.)

- All the involved SDP problems and the binary linear programming problem (21) are solved by using the Mosek solver [49] through the CVX interface in Matlab [53].
- The spectral clustering algorithm proposed in [54] is utilized to extract \mathbf{y}^c from the relation matrix \mathbf{M} .
- The feature mapping $\phi(\cdot)$ is induced from the Gaussian kernel

$$\text{Ker}(\mathbf{x}, \mathbf{x}') = \exp\left(-\frac{\|\mathbf{x} - \mathbf{x}'\|^2}{2\sigma^2}\right) \quad (23)$$

and explicitly computed by the random Fourier method [44] with $d = 50$. The width parameter σ is determined by a grid search over $\{2^{-4}, 2^{-3}, \dots, 2^4\}$ and we select the value of σ which leads to the minimal value of the objective function of the M³C problem (13).

- The value of regularization parameter β does not have a significant effect for our experiments, so it is simply fixed to 0.01.
- The parameters of termination condition are set to be $\alpha_H = 0$ and $r_{\max} = 100$, and the parameters of class balance constraint are $(\varrho_l, \varrho_u) = (0.01, 0.99)$.

For comparison purposes, the following three decomposition methods are also considered in our experiments:

1. k -medoids clustering, which directly decomposes the phase space into κ macrostates based on the set $\mathcal{S} = \{\mathbf{x}_l^t | 1 \leq l \leq L, 1 \leq t \leq M_l\}$.
2. MMC based on \mathcal{S} , where the MMC problem is solved by a mixed algorithm similar to Algorithm 1 (see Appendix C).
3. PCCA+ [26], where the implementation details are given in Appendix Appendix D.

Remark 9. k -medoids clustering and MMC can be viewed as geometric clustering methods in metastability analysis.

Remark 10. Considering the inherent randomness of the k -medoids algorithm, here we perform the k -medoids clustering (or k -medoids clustering in coarse graining steps of MMC, PCCA+ and M³C) in the following way: Repeat the k -medoids algorithm 100 times independently with random initialization and pick the solution with the minimal “within-cluster point scatter”.

6.1. Sequential unlabeled data

Here we apply M³C and other metastable state decomposition methods to sequential data which are generated by using data sets **letter**, **satellite**, **spambase**, **waveform** and **segment** from the UCI machine learning repository [55]. All data sets consist of multiple classes of instances and the pattern of each instance is represented by a multidimensional vector of real- or integer-valued features. A summary of all the data sets is in Table 1.

For each data set, we construct a sequence of unlabeled patterns as follows:

1. Generate a reversible Markov chain $\{\bar{y}_n\}_{n=1}^N$ in $\{1, \dots, \kappa\}$, where κ denotes the class number of the data set, and the transition matrix $\mathbf{P} = [P_{ij}] = [\Pr(\bar{y}_{n+1} = j | \bar{y}_n = i)] \in \mathbb{R}^{\kappa \times \kappa}$ of $\{\bar{y}_n\}$ is given by

$$\begin{aligned} \mathbf{P} &= \begin{bmatrix} 0.97 & 0.03 \\ 0.03 & 0.97 \end{bmatrix} \\ \mathbf{P} &= \begin{bmatrix} 0.97 & 0.015 & 0.015 \\ 0.025 & 0.95 & 0.025 \\ 0.02 & 0.02 & 0.96 \end{bmatrix} \\ \mathbf{P} &= \begin{bmatrix} 0.9517 & 0.0198 & 0.0138 & 0.0147 \\ 0.0198 & 0.9509 & 0.0134 & 0.0159 \\ 0.0138 & 0.0134 & 0.9535 & 0.0193 \\ 0.0147 & 0.0159 & 0.0193 & 0.9501 \end{bmatrix} \end{aligned}$$

for $\kappa = 2, 3, 4$ respectively.

2. For every $n = 1, \dots, N$, randomly select a pattern \mathbf{x}_n with class label \bar{y}_n from the data set without repetition. (This step cannot be implemented if the element number of $\{n | \bar{y}_n = i\}$ is bigger than the data size of the i -th class in the data set for some i . For such a case, we will repeat generating $\{\bar{y}_n\}$ until this step is feasible.)

Since the self-transition probabilities in transition matrices \mathbf{P} (i.e., the diagonal elements of \mathbf{P}) are all close to 1, a pattern sequence $\{\mathbf{x}_n\}$ generated as above can be viewed as a metastable processes with each class being a metastable state. Then we perform clustering of $\{\mathbf{x}_n\}$ by metastable state decomposition after removing the class labels of $\{\mathbf{x}_n\}$. Finally, the clustering accuracies of different methods are evaluated by calculating classification errors on the training data set $\{\mathbf{x}_n\}$ and the testing data set consisting of all instances not in $\{\mathbf{x}_n\}$:

$$\begin{aligned} \text{err}_{\text{train}} &= \frac{1}{N} \sum_{n=1}^N 1_{\bar{y}_n \neq y(\mathbf{x}_n)} \\ \text{err}_{\text{test}} &= \frac{1}{|\{\text{testing data}\}|} \sum_{\mathbf{x} \in \{\text{testing data}\}} 1_{\bar{y}(\mathbf{x}) \neq y(\mathbf{x})} \end{aligned} \quad (24)$$

where $\bar{y}(\mathbf{x})$ denotes the true class label of \mathbf{x} , and $y(\mathbf{x})$ denotes the predicted label given by metastable state decomposition results.

Table 2 summarizes clustering errors on the various data sets with $N = 1000$. It can be observed from the table that both PCCA+ and M³C outperform the geometric clustering methods, k -medoids and MMC, by utilizing the metastable structure in the sequential, and M³C achieves the best clustering performance among all the four methods. Moreover, considering that the clustering given by PCCA+ depend on the space discretization results (see Section 1), we report the clustering errors of PCCA+ with different numbers of discrete bins in this table. As can be seen, for most data sets, except **segment**, either the finest discretization (with 400 bins) or the coarsest discretization (with 50 bins) cannot lead to the best PCCA+ clustering results, which demonstrates the sensitivity of PCCA+ to the choice of space discretization.

Table 1: Summary of the data sets

	size	pattern dimension	number of classes ^{a)} (κ)
letter	1555	17	2
satellite	2236	36	2
spambase	4601	57	2
waveform	5000	21	3
segment	1320	19	4

^{a)} For data sets which contain more than κ classes, we only use their subsets consisting of the first κ classes.

Table 2: Means and standard deviations of clustering errors (in percent) calculated over 20 independent experiments of various data sets

		k -medoids	MMC	PCCA+ (50 bins)	PCCA+ (200 bins)	PCCA+ (300 bins)	PCCA+ (400 bins)	M ³ C
letter	err _{train}	8.6306 ± 3.0850	7.0090 ± 3.2752	2.2450 ± 1.0128	0.5450 ± 0.1849	0.4450 ± 0.2585	0.5950 ± 0.2837	0.1100 ± 0.0852
	err _{test}	8.6400 ± 3.0025	7.3600 ± 3.6059	2.7207 ± 1.4567	1.1171 ± 0.5746	0.7658 ± 0.5871	1.0270 ± 0.6299	0.2342 ± 0.1963
satellite	err _{train}	2.3503 ± 0.8560	2.3058 ± 0.8616	0.7727 ± 0.2905	0.6600 ± 0.2741	0.7600 ± 0.2604	0.8600 ± 0.2501	0.0900 ± 0.0912
	err _{test}	6.7950 ± 1.3069	6.6450 ± 1.4365	1.1950 ± 0.3348	0.7727 ± 0.3457	0.9102 ± 0.3803	1.0720 ± 0.5436	0.3196 ± 0.1325
spambase	err _{train}	36.8773 ± 1.8360	22.5923 ± 9.7192	23.6000 ± 9.2388	25.7450 ± 13.4768	22.7950 ± 12.4952	28.3671 ± 8.2107	8.5296 ± 1.2141
	err _{test}	45.0150 ± 4.2245	23.7650 ± 7.4026	24.7362 ± 7.8620	27.1355 ± 9.7611	23.9572 ± 8.3935	30.2900 ± 15.3507	12.2350 ± 1.0338
waveform	err _{train}	46.6212 ± 2.8506	34.1600 ± 16.3716	23.5425 ± 2.6599	21.5525 ± 2.9225	26.1075 ± 8.1388	30.3725 ± 13.9271	15.0550 ± 7.1295
	err _{test}	47.4550 ± 2.0623	37.4900 ± 16.0950	27.2483 ± 3.7676	27.6700 ± 4.5708	33.6117 ± 9.91157	36.5450 ± 13.2638	22.2675 ± 10.4104
segment	err _{train}	21.2417 ± 11.3240	8.1050 ± 3.9986	5.4500 ± 1.0273	2.6050 ± 0.4729	2.4850 ± 0.8845	2.3400 ± 0.6652	1.3750 ± 0.3059
	err _{test}	31.9750 ± 7.9013	18.3234 ± 18.1635	14.9662 ± 12.2071	10.2918 ± 12.3009	10.5916 ± 12.2503	9.1230 ± 9.8576	2.5392 ± 1.6581

6.2. Diffusion models

We now consider two examples of time-reversible diffusion processes, denoted by Model I and Model II, which can be described by two dimensional Fokker-Planck equations (see Appendix E for details).

For metastable state decomposition of Model I, we generate 10 trajectories by 10 independent simulations with time length 80, sample interval $\Delta t = 0.2$ and initial states \mathbf{x}_0 distributed according to an uniform distribution on $[-1.5, 1.5]^2$. Fig. 3 shows the potential energy and simulation trajectories, where $\mathbf{x}_t = (x_t^{(1)}, x_t^{(2)})$ denotes the system state at time t , the potential function $V(\mathbf{x})$ is defined by $\pi(\mathbf{x}) \propto \exp(-V(\mathbf{x}))$ and $\pi(\mathbf{x})$ is the equilibrium distribution $\lim_{t \rightarrow \infty} p(\mathbf{x}_t = \mathbf{x})$. We can observe that Model I has 6 potential wells, and the energy barrier between the “upper” wells (with $x^{(2)} > 0$) and the “lower” ones (with $x^{(2)} < 0$) can be easily crossed. Therefore, the phase space of Model I can be decomposed into 3 metastable states with each one containing an upper and a lower potential well. Fig. 4 displays the decomposition results of all four methods with $\kappa = 3$ by using the trajectory data shown in Fig. 3b, where the bin number of PCCA+ is set to be 10. It is obvious that M³C and PCCA+ accurately identify the three metastable states, while the macrostates given by k -medoids and MMC do not exhibit strong metastability although the decomposition results of the latter two methods are “reasonable” in the sense of geometric clustering. This shows the limitation of geometric clustering methods in the case that the spatial structure of metastable states does not only depend on the shape of equilibrium state distribution function.

Note that the decomposition result displayed in Fig. 4c might not be the

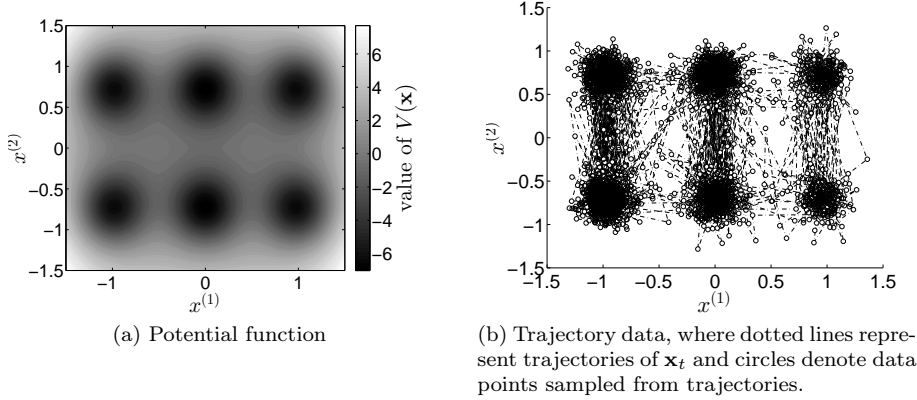


Figure 3: Illustration of Model I.

global optima of the MMC problem. It is natural to ask if MMC can correctly find the metastable states by choosing a better initial solution for the local search procedure. In order to answer this question, we solve the MMC problem by the local search algorithm in [43] starting from the decomposition provided by M^3C . Fig. 5 shows the corresponding decomposition result, which is very similar to that obtained by M^3C and PCCA+. However, the objective function value of this decomposition in the MMC problem is 0.0652, which is larger than the objective function value 0.0496 of the decomposition shown in Fig. 4c. This indicates that MMC prefer the decomposition in Fig. 4c to that in Fig. 5, although the latter one is better for metastability analysis.

Moreover, we also perform the local search algorithm to solve the M^3C problem with random initialization, and Fig. 6 plots the optimization result. As observed from the figure, the randomly generated initial solution leads to the algorithm getting stuck in a local optimum. (The optimal objective function values of the M^3C problem obtained by the local search with random initialization and the mixed-algorithm proposed in Section 5.3 are 0.1553 and 0.0967 separately.) It shows that the local search algorithm proposed in Section 5.2 is sensitive to initial conditions, and some heuristic method (e.g., the global search algorithm presented in this paper) is needed to provide a satisfactory initial solution.

The potential energy of Model II is shown in Fig. 7a. We generate 50 trajectories in the state space of Model II in order to test the metastable state decomposition methods (see Fig 7b), where the time length of each trajectory is 1, the sample interval is $\Delta t = 0.02$ and the initial states are uniformly sampled from $[-2, 2]^2$. It is easy to see that Model II has three metastable states formed by the three potential wells.

Fig. 8 summarizes the decomposition results with $\kappa = 3$. Figs. 8b and 8c show that k -medoids and MMC fail to identify the three metastable states in

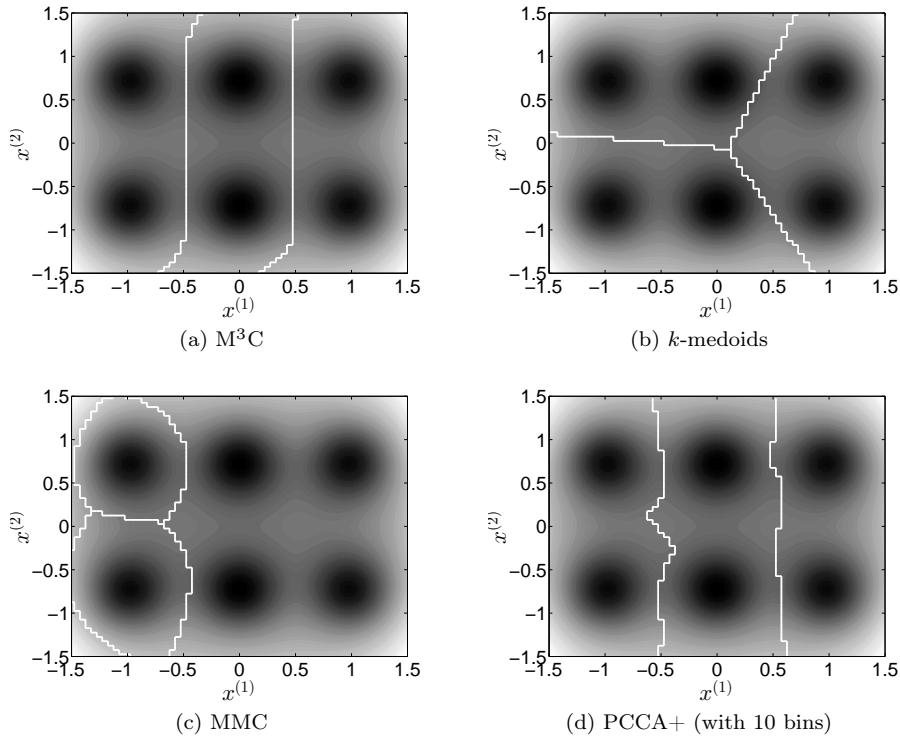


Figure 4: Decomposition results of Model I, where white lines represent boundaries between macrostates. The boundaries are computed by the finite element method with mesh size 0.05×0.05 .

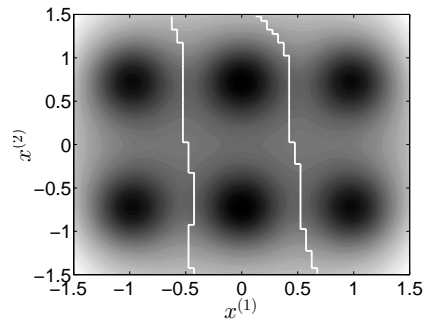


Figure 5: Decomposition result of Model I obtained by the local search based MMC with initial solution given by M^3C .

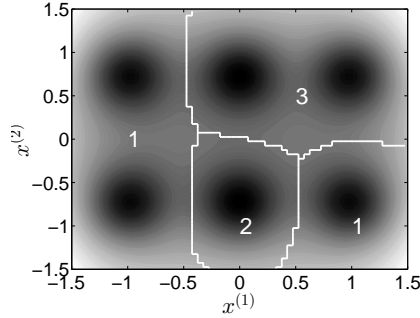


Figure 6: Decomposition result of Model I obtained by the local search based M³C with random initialization.

Model II due to the large difference between the empirical data distribution and the equilibrium distribution. It is interesting to see from Fig. 8d that PCCA+ (with 20 discrete bins) also gives an undesired decomposition. We now analyze why PCCA+ fails in this example. Note that there is a low energy barrier at the center of the right potential well (see the rectangular region with the dashed line in Fig. 7 and its magnified picture shown in Fig. 9), which can be easily crossed for equilibrium simulations. But the trajectory data used in the above is very far away from the global equilibrium due to short simulation lengths. So only a small number of transitions between discrete bins of PCCA+ are observed around this region, and the PCCA+ assigns these bins to different metastable states. In all the four methods, M³C is the only method that get correct metastable state decomposition by utilizing both the geometric and the dynamical information, and it avoids splitting the right potential well into two metastable states as PCCA+ because such a decomposition leads to a small margin between metastable boundaries.

Finally, we repeat the above numerical experiments of Model I and Model II for 20 times and utilize the following quantities to evaluate and compare the performance of different decomposition methods quantitatively:

1. $Q = \sum_{k=1}^{\kappa} P_{kk}(\Delta t)$, where Δt denotes the sample interval and

$$P_{ij}(\tau) = \lim_{t \rightarrow \infty} \Pr(\mathbf{x}_{t+\tau} \in \text{metastable state } j | \mathbf{x}_t \in \text{metastable state } i) \quad (25)$$

denotes the transition probability between metastable states with lagtime τ . It is clear that Q can measure the metastability of a system and a decomposition with strongly metastability will result in a large Q close to κ [32].

2. Implied timescale $\text{ITS}_i(\tau) = -\tau / \ln \lambda_i(\tau)$ with $i > 1$, where $\lambda_i(\tau)$ denotes the i -th largest eigenvalue of transition probability matrix $\mathbf{P}(\tau) = [P_{ij}(\tau)]$. (The first implied timescale $\text{ITS}_1(\tau) \equiv \infty$) It can be proved that the value of $\text{ITS}_i(\tau)$ is a constant independent of τ and equal to the

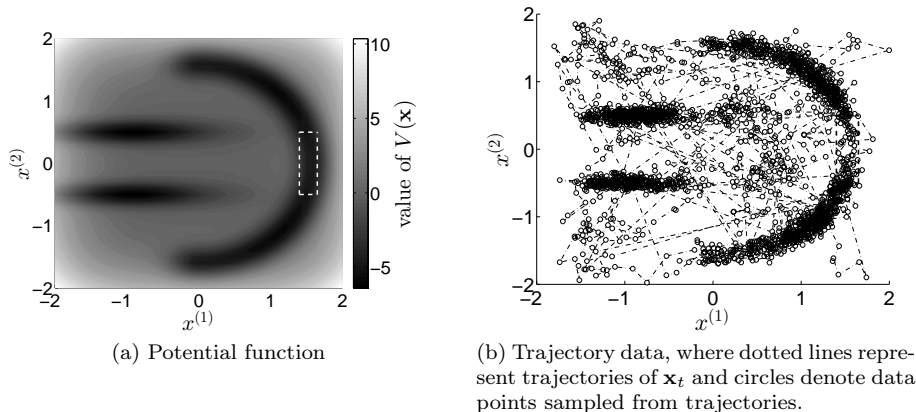


Figure 7: Illustration of Model II, where the rectangular with dashed lines shows the region $[1.4, 1.65] \times [-0.5, 0.5]$ of a low energy barrier within the right potential well.

dominant relaxation timescales of the original system if the transitions between metastable states are exactly Markovian [12, 16]. Thus, we can check if a Markov chain on metastable states can accurately approximate the system dynamics through comparing implied timescales with different τ .

Remark 11. We run a long simulation with time length 10^4 to estimate values of $P_{ij}(\tau)$ for each model. Furthermore, for convenience of comparison, we use the finely discretized Markov state models with 50 states to estimate the true relaxation timescales of Model I and Model II. The detailed estimation algorithms are given in [5].

Table 3 and Figs. 10 and 11 summarize the values of Q and implied timescales given by different decomposition methods, including the PCCA+ method with different bin numbers. The table and figures also demonstrate the superior performance of M^3C . It is worth pointing out that in 9 out of 20 experiments of Model II, PCCA+ wrongly decomposes the right potential well into two metastable states (with any bin number), whereas M^3C gives the “ideal” decomposition in all the 20 experiments. Moreover, as can be seen from the figures, the implied timescales obtained from M^3C converge fast and are very close to the relaxation timescales estimated by finely discretized Markov state models, which implies that the essential dynamical properties of Model I and Model II can be accurately captured by 3-state Markov models using the metastable states identified by M^3C .

6.3. Molecular dynamics simulations

We consider in this section the metastable state decomposition problem of molecular dynamics simulation models of alanine dipeptide and deca-alanine.

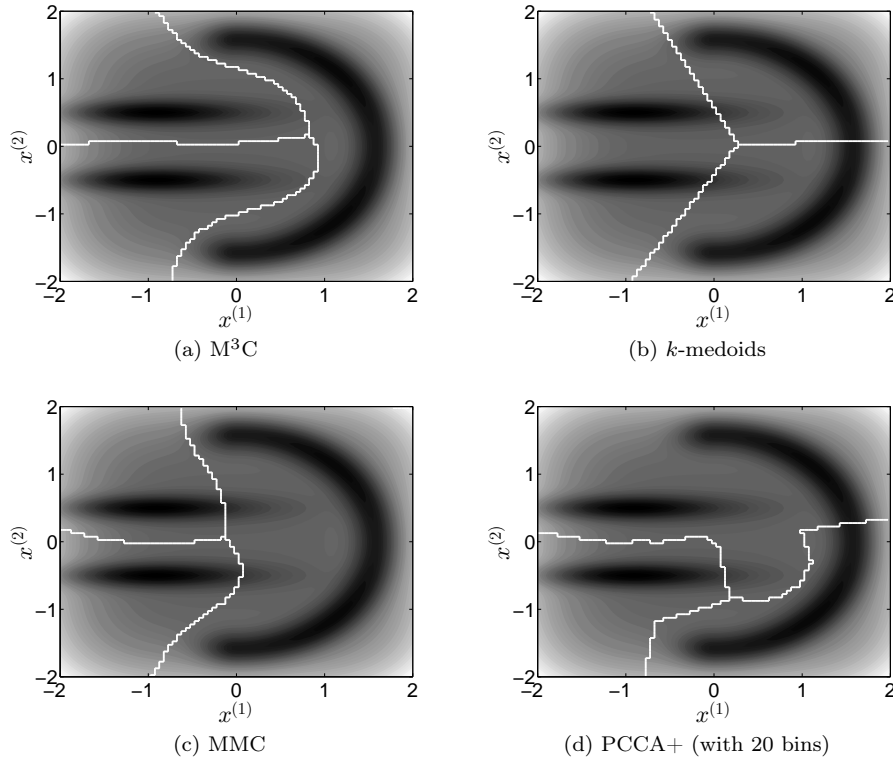


Figure 8: Decomposition results of Model II, where white lines represent boundaries between macrostates. The boundaries are computed by the finite element method with mesh size 0.05×0.05 .

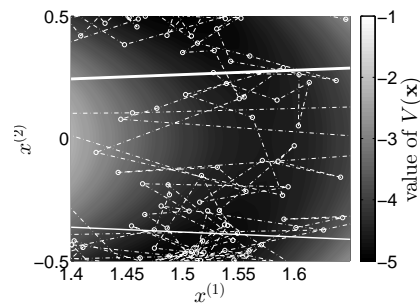


Figure 9: PCCA+ decomposition result of Model II in the area $[1.4, 1.65] \times [-0.5, 0.5]$, where dotted lines represent trajectories, circles denote data points sampled from trajectories, solid lines show boundaries of discrete bins obtained by space discretization, and the upper boundary is chosen to be the metastable state boundary by the PCCA+ algorithm.

Table 3: Means and standard deviations of Q values calculated over 20 independent experiments of Models I and II

	k -medoids	MMC	PCCA+ (6 bins)	PCCA+ (10 bins)	PCCA+ (20 bins)	PCCA+ (30 bins)	PCCA+ (40 bins)	M ³ C
Model I	2.8138 ± 0.0317	2.8142 ± 0.0244	2.9603 ± 0.0170	2.9637 ± 0.0011	2.9628 ± 0.0017	2.9619 ± 0.0027	2.9613 ± 0.0021	2.9641 ± 0.0005
Model II	2.9579 ± 0.0031	2.9832 ± 0.0116	2.9681 ± 0.0211	2.9666 ± 0.0161	2.9676 ± 0.0173	2.9655 ± 0.0187	2.9600 ± 0.0285	2.9882 ± 0.0024

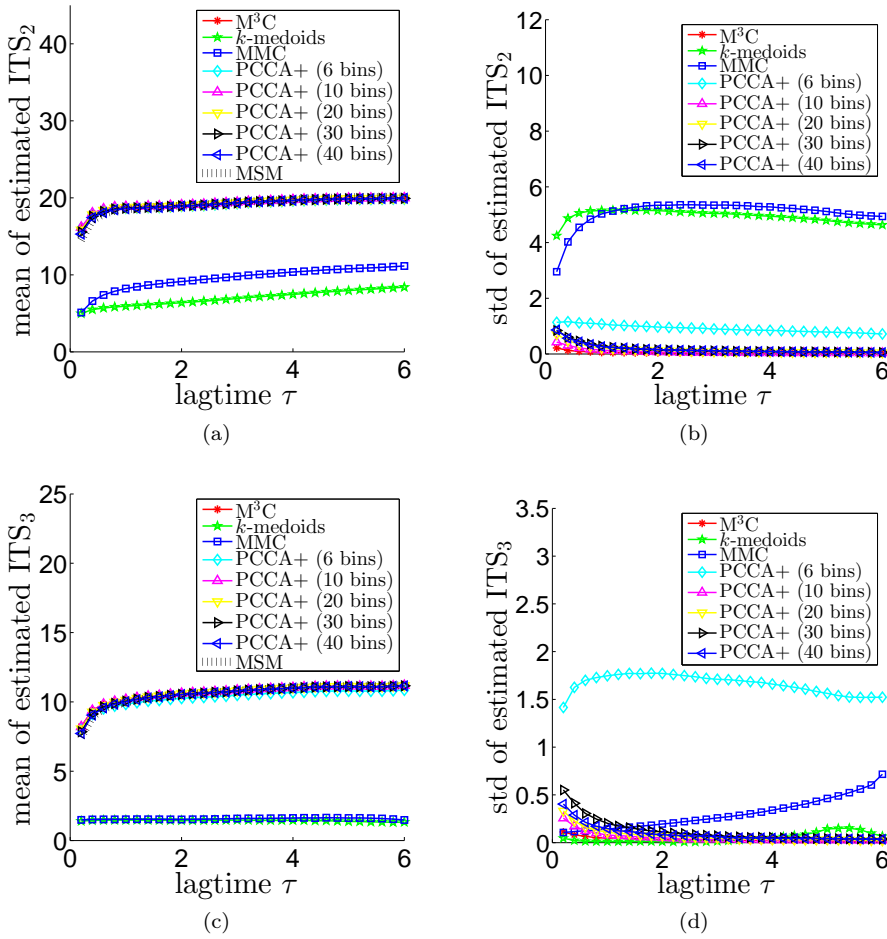


Figure 10: Means and standard deviations of estimated implied timescales of Model I obtained by different decomposition methods, where dotted lines indicate estimates of the second and third relaxation timescales of Model I computed by 50-state Markov state models.

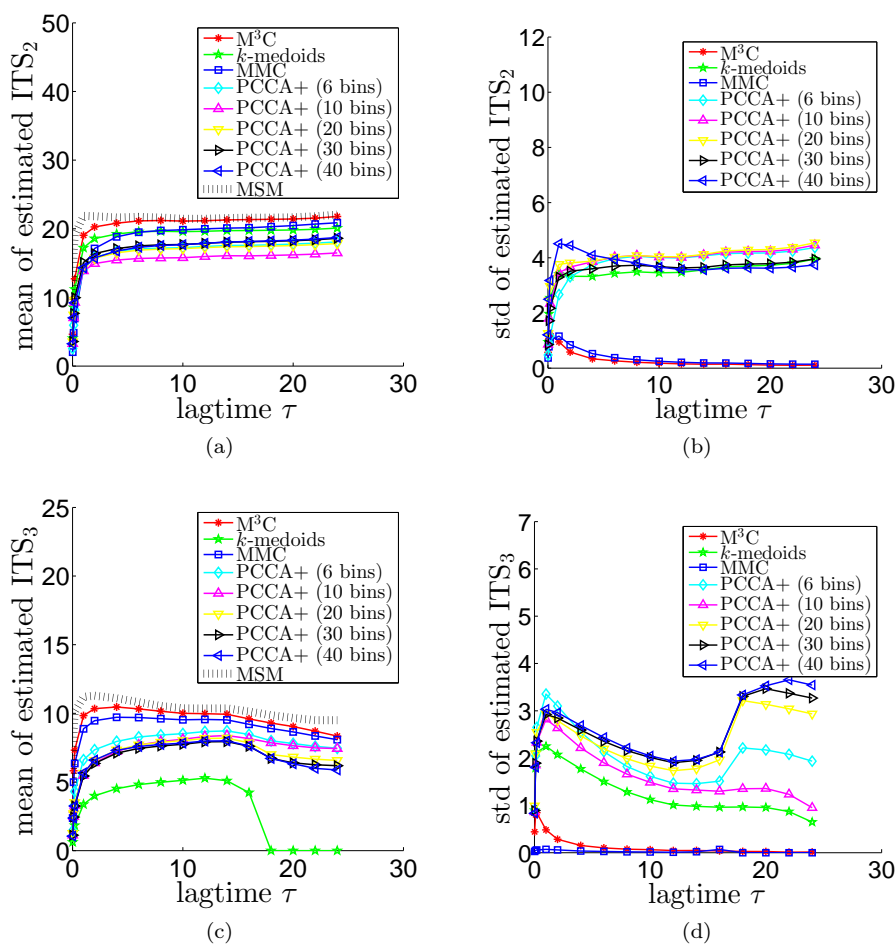


Figure 11: Means and standard deviations of estimated implied timescales of Model II obtained by different decomposition methods, where dotted lines indicate estimates of the second and third relaxation timescales of Model II computed by 50-state Markov state models. (The implied timescale value is set to be zero if the corresponding eigenvalue of the transition probability matrix is zero or negative.)

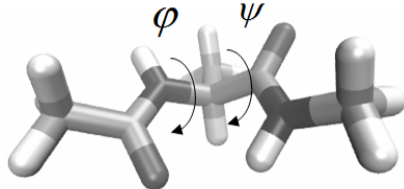


Figure 12: Illustration of the structure of alanine dipeptide

Alanine dipeptide (sequence acetyl-alanine-methylamide) is a small molecule which consists of two alanine amino acid units. The structural and dynamical properties of this molecule have been thoroughly studied, and its conformation space (phase space) can be conveniently described by two backbone dihedral angles φ and ψ (see Fig. 12). Deca-alanine is a small peptide composed of 10 alanine residues, and its configuration can be described by 18 backbone dihedral angles. We perform twenty simulations of 200ns of molecular dynamics of alanine dipeptide with sample interval 20ps and six 500ns molecular dynamics simulations of deca-alanine with sample interval 100ps (The detailed simulation model is given in [56]).

The metastable state decomposition methods are applied to each simulation trajectory ($\kappa = 3$ for alanine dipeptide and $\kappa = 2$ for deca-alanine), and the corresponding Q values and implied timescales are calculated from all the other trajectories of the same molecule. Moreover, considering the periodicity of angular data, we represent the molecular state as a vector \mathbf{x} consisting of sin/cos of the dihedral angles in experiments.

Fig. 13a shows the potential function of alanine dipeptide in the space of (φ, ψ) and the three metastable states which can be manually identified according to experience, and data points sampled from one simulation trajectory are displayed in Fig. 13b. The decomposition results of the simulation trajectory are plotted in Fig. 14. As can be seen, k -medoids and MMC fail to indentify the metastable structure of alanine dipeptide, and the decompositions obtained by PCCA+ and M³C are consistent with the manual decomposition. Table 4 and Fig. 15 summarize Q values and implied timescales given by decomposition results of simulation trajectories of alanine dipeptide. It can be observed that PCCA+ and M³C performs significantly better than the geometric clustering methods k -medoids and MMC. M³C achieves the similar average Q values and implied timescales as PCCA+, but the corresponding standard deviations of M³C are lower than that of PCCA+, which shows M³C has more stable performance for this molecular dynamics simulation model.

The decomposition results of deca-alanine are displayed in Table 4 and Fig. 16. The Q values obtained by M³C are significantly smaller than that

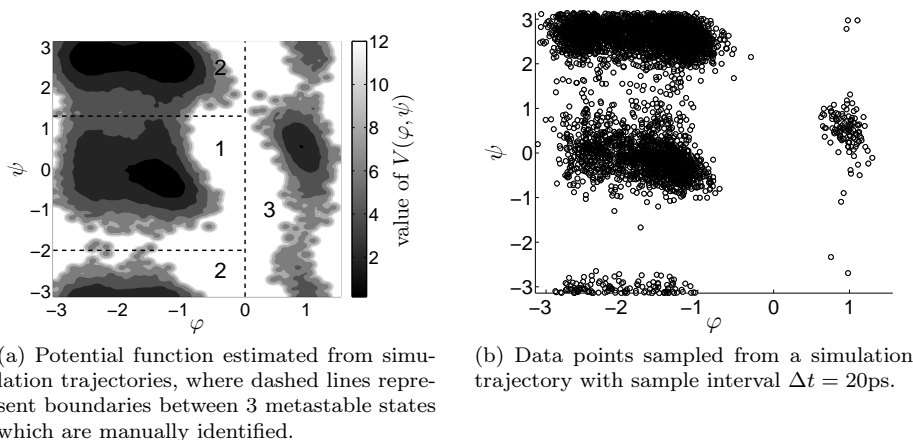


Figure 13: Illustration of the molecular dynamics simulation of alanine dipeptide

Table 4: Means and standard deviations of Q values calculated over 10 independent experiments of alanine dipeptide and 6 independent experiments of deca-alanine

	k -medoids	MMC	PCCA+ (100 bins)	PCCA+ (200 bins)	PCCA+ (300 bins)	PCCA+ (400 bins)	PCCA+ (500 bins)	M ³ C
alanine dipeptide	1.7655 ± 0.0027	2.1521 ± 0.5060	2.7360 ± 0.0077	2.7381 ± 0.0018	2.7367 ± 0.0059	2.7340 ± 0.0037	2.7328 ± 0.0052	2.7397 ± 0.0003
deca-alanine	1.8113 ± 0.0502	1.8819 ± 0.0454	1.9033 ± 0.0292	1.8904 ± 0.0402	1.8894 ± 0.0815	1.9227 ± 0.0238	1.8896 ± 0.0764	1.9592 ± 0.0038

given by the other methods. In contrast to alanine dipeptide, the kinetics of deca-alanine is much more complicated and it is difficult to accurately estimate the relaxation timescales. In [56], a lower bound 6.5ns for the second relaxation timescale is given. Moreover, according to the variational principle [57], the second implied timescale obtained from a metastable state decomposition is always smaller than the true one if there is no statistical noise. So we can conclude from Fig. 16 that M³C gives more accurate estimate of ITS₂ than the other methods for this molecular dynamics model.

7. Conclusion

Large margin methods have turned out to be an effective and robust approach for supervised and unsupervised learning problems. In this paper, we apply the large margin principle to the metastable state decomposition problem, and propose a *maximum margin metastable clustering* (M³C) method to identify metastable states of complex stochastic systems. The key step is to design a large margin metastable constraint (9) by combining the metastability criterion and large margin criterion, where we assign a class label to each transition pair in trajectories instead of a single data point. Then the error of metastable state decomposition can be expressed by the misclassification loss function in large margin learning, and a lot of well developed computational techniques for large

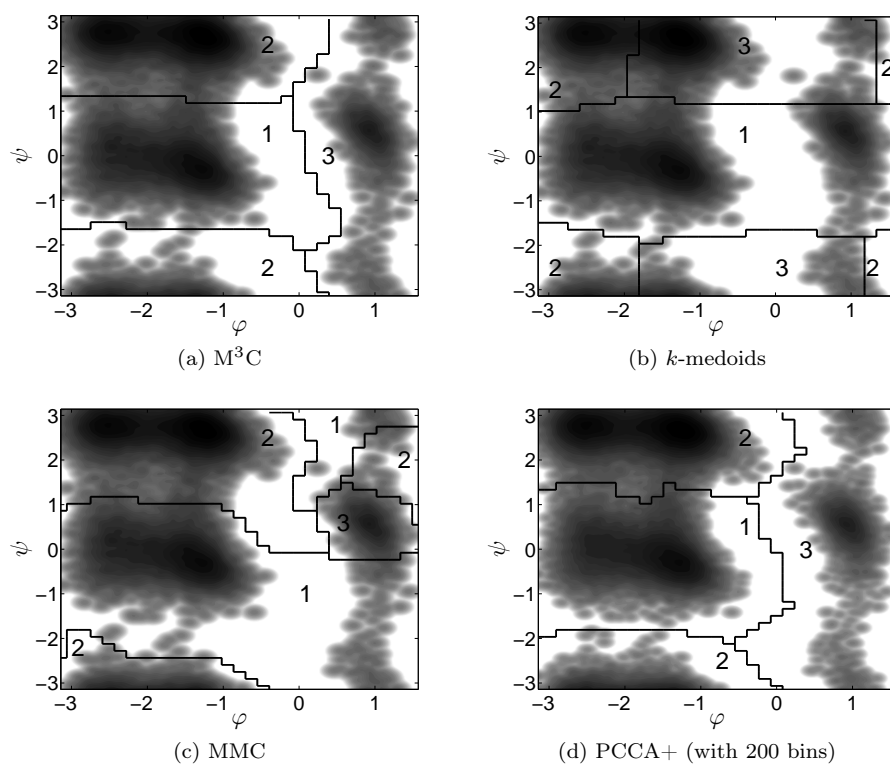


Figure 14: Decomposition results of the simulation model of alanine dipetide, where black lines represent boundaries between macrostates. The boundaries are computed by the finite element method with mesh size $0.05\pi \times 0.05\pi$.

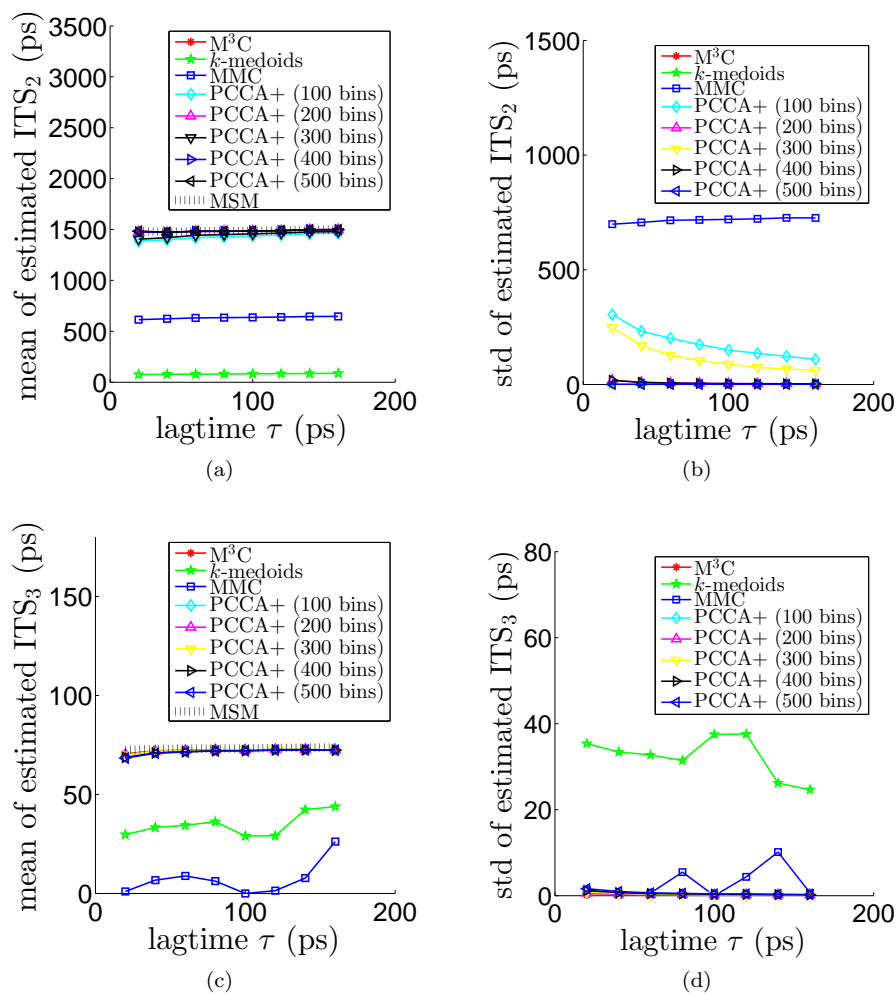


Figure 15: Means and standard deviations of estimated implied timescales of alanine dipeptide obtained by different decomposition methods, where dotted lines indicate estimates of the second and third relaxation timescales of alanine dipeptide computed by 500-state Markov state models.

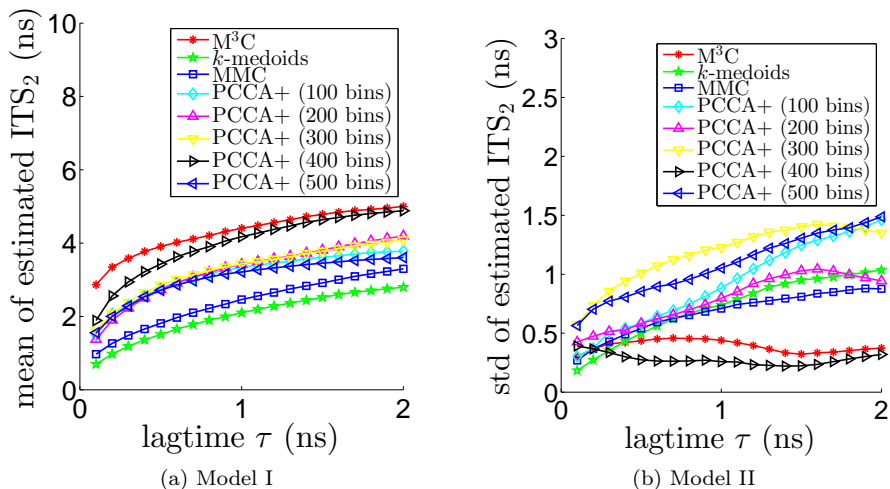


Figure 16: Means and standard deviations of estimated implied timescales of deca-alanine obtained by different decomposition methods.

margin learning, such as kernel based feature mapping and convex relaxation, can be utilized. Moreover, we present a hybrid optimization algorithm which mixes global search and local search strategies to solve M³C problems with large-scale data sets. In contrast to previous metastable state decomposition methods including geometric clustering methods and kinetic clustering methods, the M³C method can effectively utilize both the geometric information and the dynamical information provided by trajectories without pre-discretization in space, and our experimental analysis reveal that the M³C method yields more accurate and robust decomposition results than traditional geometric and kinetics clustering methods in most cases.

The major drawback of M³C is that the computing burden will be heavy for very large data set, because it need to iteratively solve an SVM-like problem. In the future, we will use some modern SVM techniques such as Pegasos[58] and core vector machine[59] to improve the efficiency of M³C. Moreover, we will investigate how to extend our method to the problem of slow process decomposition of metastable systems [57, 60] by incorporating the distance metric learning technique [61] so that it can not only detect metastable states but also extract dominant dynamical features from simulation and experimental data.

Acknowledgments

This work is supported by the Deutsche Forschungsgemeinschaft (DFG) under grant Number WU 744/1-1, and the author would like to thank Feliks Nüske (FU Berlin) for providing the molecular dynamics simulation data.

Appendix A. Proof of equivalence between (9) and (12)

Suppose first that (12) holds. Substituting $(\bar{k}, \underline{k}) = (k, y_n)$ and $(\bar{k}, \underline{k}) = (y_n, k)$ into (12), we can get

$$\begin{aligned} & \left(\mathbf{w}_{y_n y_n}^\top - \mathbf{w}_{\bar{k} \underline{k}}^\top \right) \phi(\bar{\mathbf{x}}_n, \mathbf{x}_n) + \left(b_{y_n y_n} - b_{\bar{k} \underline{k}} \right) + 1_{y_n = \bar{k} = \underline{k}} \\ &= \left(\mathbf{w}_{y_n}^\top - \mathbf{w}_k^\top \right) \phi(\bar{\mathbf{x}}_n) + (b_{y_n} - b_k) + 1_{y_n = k} \\ &\geq 1 \end{aligned} \quad (\text{A.1})$$

and

$$\begin{aligned} & \left(\mathbf{w}_{y_n y_n}^\top - \mathbf{w}_{\bar{k} \underline{k}}^\top \right) \phi(\bar{\mathbf{x}}_n, \mathbf{x}_n) + \left(b_{y_n y_n} - b_{\bar{k} \underline{k}} \right) + 1_{y_n = \bar{k} = \underline{k}} \\ &= \left(\mathbf{w}_{y_n}^\top - \mathbf{w}_k^\top \right) \phi(\mathbf{x}_n) + (b_{y_n} - b_k) + 1_{y_n = k} \\ &\geq 1 \end{aligned} \quad (\text{A.2})$$

So (12) is a sufficient condition for (9).

We now show the necessity of (12) for (9). Substituting $k = \bar{k}$ and $k = \underline{k}$ into the two inequalities in (9), respectively, yields

$$\left(\mathbf{w}_{y_n y_n}^\top - \mathbf{w}_{\bar{k} \underline{k}}^\top \right) \phi(\bar{\mathbf{x}}_n, \mathbf{x}_n) + \left(b_{y_n y_n} - b_{\bar{k} \underline{k}} \right) + (1_{y_n = \bar{k}} + 1_{y_n = \underline{k}} - 1) \geq 1 \quad (\text{A.3})$$

Note that

$$1_{y_n = \bar{k}} + 1_{y_n = \underline{k}} - 1 = \begin{cases} 1, & y_n = \bar{k} = \underline{k} \\ 0, & y_n \in \{\bar{k}, \underline{k}\}, \bar{k} \neq \underline{k} \\ -1, & \text{otherwise} \end{cases} \quad (\text{A.4})$$

and

$$1_{y_n = \bar{k} = \underline{k}} = \begin{cases} 1, & y_n = \bar{k} = \underline{k} \\ 0, & \text{otherwise} \end{cases} \quad (\text{A.5})$$

Therefore,

$$\begin{aligned} & \left(\mathbf{w}_{y_n y_n}^\top - \mathbf{w}_{\bar{k} \underline{k}}^\top \right) \phi(\bar{\mathbf{x}}_n, \mathbf{x}_n) + \left(b_{y_n y_n} - b_{\bar{k} \underline{k}} \right) + 1_{y_n = \bar{k} = \underline{k}} \\ &\geq \left(\mathbf{w}_{y_n y_n}^\top - \mathbf{w}_{\bar{k} \underline{k}}^\top \right) \phi(\bar{\mathbf{x}}_n, \mathbf{x}_n) + \left(b_{y_n y_n} - b_{\bar{k} \underline{k}} \right) + (1_{y_n = \bar{k}} + 1_{y_n = \underline{k}} - 1) \\ &\geq 1 \end{aligned} \quad (\text{A.6})$$

From the above, we can conclude that (12) is equivalent to (9).

Appendix B. Proof of Theorem 5

Let us start with the case that all labels \mathbf{y}^c in (14) are given. In this case, the coarse-grained M³C problem (14) is reduced to a simple quadratic programming problem:

$$\begin{aligned} & \min_{\mathbf{W}, \xi^c} \quad \frac{1}{2} \beta \|\mathbf{W}\|^2 + \mathbf{c}^\top \xi^c \\ & \text{s.t.} \quad \forall n = 1, \dots, N^c, \quad \forall \bar{k}, \underline{k} = 1, \dots, \kappa, \\ & \quad \left(\mathbf{w}_{y_n^c y_n^c}^\top - \mathbf{w}_{\bar{k} \underline{k}}^\top \right) \phi(\bar{\mathbf{x}}_n^c, \mathbf{x}_n) + 1_{y_n^c = \bar{k} = \underline{k}} \geq 1 - \xi_n^c, \end{aligned} \quad (\text{B.1})$$

For the sake of convenience, here we let \mathbf{e}_k denote a κ dimensional vector with only the k -th element being 1 and others 0, and define a matrix $\mathbf{B} \in \mathbb{R}^{2\kappa \times \kappa^2}$ as

$$\mathbf{B} = \begin{bmatrix} \bar{\mathbf{B}} \\ \mathbf{B} \end{bmatrix} = \begin{bmatrix} \mathbf{e}_1 & \mathbf{e}_2 & \cdots & \mathbf{e}_\kappa & \mathbf{e}_1 & \mathbf{e}_1 & \cdots & \mathbf{e}_\kappa \\ \mathbf{e}_1 & \mathbf{e}_2 & \cdots & \mathbf{e}_\kappa & \mathbf{e}_2 & \mathbf{e}_3 & \cdots & \mathbf{e}_{\kappa-1} \end{bmatrix} \quad (\text{B.2})$$

i.e., each column of \mathbf{B} is an element of $\{(\mathbf{e}_i^\top, \mathbf{e}_j^\top)^\top | i, j \in [1, \kappa]\}$ and the first κ columns of \mathbf{B} is equal to $[\mathbf{I} \ \mathbf{I}]^\top$, where $\bar{\mathbf{B}}, \mathbf{B} \in \mathbb{R}^{\kappa \times \kappa^2}$ are two submatrices consisting of the first κ and the last κ rows of \mathbf{B} .

By introducing a dual variable $\boldsymbol{\Lambda} \in \mathbb{R}^{N^c \times \kappa^2}$ and using (15) and (B.2), the Lagrangian of (B.1) can be written as

$$\begin{aligned} \mathcal{L} &= \frac{1}{2}\beta \|\mathbf{W}\|^2 + \mathbf{c}^\top \boldsymbol{\xi}^c - \text{tr}(\mathbf{D}^\top \text{diag}(\boldsymbol{\Lambda} \mathbf{1}) (\bar{\mathbf{X}} + \mathbf{X}) \mathbf{W}^\top) \\ &\quad - \text{tr}([\ \boldsymbol{\Lambda}^\top \mathbf{D} \ \mathbf{0} \mathbf{0}^\top \]) + \text{tr}(\boldsymbol{\Lambda}^\top (\bar{\mathbf{X}} \mathbf{W}^\top \bar{\mathbf{B}} + \mathbf{X} \mathbf{W}^\top \mathbf{B})) \\ &\quad + (\mathbf{1} - \boldsymbol{\xi}^c)^\top \boldsymbol{\Lambda} \mathbf{1} \end{aligned} \quad (\text{B.3})$$

where $\bar{\mathbf{X}} = (\phi(\bar{\mathbf{x}}_1^c), \dots, \phi(\bar{\mathbf{x}}_{N^c}^c))^\top \in \mathbb{R}^{N^c \times d}$ and $\mathbf{X} = (\phi(\mathbf{x}_1^c), \dots, \phi(\mathbf{x}_{N^c}^c))^\top \in \mathbb{R}^{N^c \times d}$. Setting the derivatives of the Lagrangian (B.3) with respect to \mathbf{W} and $\boldsymbol{\xi}^c$ to zero, and adding the constraint $\boldsymbol{\Lambda} \geq 0$, we obtain the following dual problem of (B.1):

$$\begin{aligned} \max_{\boldsymbol{\Lambda}} &\quad -\frac{1}{2\beta} \text{tr}([\ \bar{\mathbf{B}} \boldsymbol{\Lambda}^\top \ \mathbf{B} \boldsymbol{\Lambda}^\top \] \mathbf{K} [\ \bar{\mathbf{B}} \boldsymbol{\Lambda}^\top \ \mathbf{B} \boldsymbol{\Lambda}^\top \]^\top) \\ &\quad + \frac{1}{\beta} \text{tr}(\mathbf{D}^\top \mathbf{C} [\ \mathbf{I} \ \mathbf{I} \] \mathbf{K} [\ \bar{\mathbf{B}} \boldsymbol{\Lambda}^\top \ \mathbf{B} \boldsymbol{\Lambda}^\top \]^\top) \\ &\quad - \text{tr}([\ \boldsymbol{\Lambda}^\top \mathbf{D} \ \mathbf{0} \mathbf{0}^\top \]) - \frac{1}{2\beta} \text{tr}(\mathbf{MCK}^s \mathbf{C}) + \mathbf{1}^\top \mathbf{c} \\ \text{s.t.} &\quad \boldsymbol{\Lambda} \mathbf{1} = \mathbf{1}, \\ &\quad \boldsymbol{\Lambda} \geq 0. \end{aligned} \quad (\text{B.4})$$

where

$$\mathbf{K} = \begin{bmatrix} \mathbf{K}^{(1,1)} & \mathbf{K}^{(1,2)} \\ \mathbf{K}^{(2,1)} & \mathbf{K}^{(2,2)} \end{bmatrix} \quad (\text{B.5})$$

$$\mathbf{K}^s = \mathbf{K}^{(1,1)} + \mathbf{K}^{(1,2)} + \mathbf{K}^{(2,1)} + \mathbf{K}^{(2,2)} \quad (\text{B.6})$$

and

$$\mathbf{K}^{(1,1)} = \bar{\mathbf{X}}^\top \bar{\mathbf{X}}, \mathbf{K}^{(1,2)} = \bar{\mathbf{X}}^\top \mathbf{X}, \mathbf{K}^{(2,1)} = \mathbf{X}^\top \bar{\mathbf{X}}, \mathbf{K}^{(2,2)} = \mathbf{X}^\top \mathbf{X} \quad (\text{B.7})$$

Putting (B.4) into the form of a standard quadratic programming problem, we have

$$\begin{aligned} \max_{\boldsymbol{\Lambda}} &\quad -\frac{1}{2\beta} \text{vec}(\boldsymbol{\Lambda})^\top \mathbf{P} \text{vec}(\boldsymbol{\Lambda}) + \mathbf{q}^\top \text{vec}(\boldsymbol{\Lambda}) - \frac{1}{2\beta} \text{tr}(\mathbf{MCK}^s \mathbf{C}) + \mathbf{1}^\top \mathbf{c} \\ \text{s.t.} &\quad (\mathbf{1}^\top \otimes \mathbf{I}) \text{vec}(\boldsymbol{\Lambda}) = \mathbf{1}, \\ &\quad \text{vec}(\boldsymbol{\Lambda}) \geq 0. \end{aligned} \quad (\text{B.8})$$

where

$$\begin{aligned} \mathbf{P} &= (\bar{\mathbf{B}}^\top \bar{\mathbf{B}}) \otimes \mathbf{K}^{(1,1)} + (\bar{\mathbf{B}}^\top \mathbf{B}) \otimes \mathbf{K}^{(1,2)} \\ &\quad + (\mathbf{B}^\top \bar{\mathbf{B}}) \otimes \mathbf{K}^{(2,1)} + (\mathbf{B}^\top \mathbf{B}) \otimes \mathbf{K}^{(2,2)} \end{aligned} \quad (\text{B.9})$$

and

$$\begin{aligned} \mathbf{q} = & \text{vec} \left(\frac{1}{\beta} \left(\mathbf{K}^{(1,1)} + \mathbf{K}^{(2,1)} \right)^\top \mathbf{C}^\top \mathbf{D} \bar{\mathbf{B}} \right. \\ & \left. + \frac{1}{\beta} \left(\mathbf{K}^{(1,2)} + \mathbf{K}^{(2,2)} \right)^\top \mathbf{C}^\top \mathbf{D} \mathbf{B} - \left[\mathbf{D} \quad \mathbf{0} \mathbf{0}^\top \right] \right) \end{aligned} \quad (\text{B.10})$$

(The definition of $\text{vec}(\cdot)$ is given in the list of notation.) According to Lemma 12 and the strong duality theorem [62], we can conclude that (B.1) has the same minimum with the following optimization problem:

$$\begin{aligned} \min_{\boldsymbol{\alpha}, \mathbf{v}, \boldsymbol{\theta}} \quad & \frac{1}{2} \boldsymbol{\theta}^\top \boldsymbol{\theta} - \mathbf{c}^\top \boldsymbol{\alpha} - \frac{1}{2\beta} \text{tr}(\mathbf{MCK}^s \mathbf{C}) + \mathbf{1}^\top \mathbf{c} \\ \text{s.t.} \quad & \mathbf{q} + (\mathbf{1} \otimes \mathbf{I}) \boldsymbol{\alpha} + \mathbf{v} + \mathbf{R} \boldsymbol{\theta} = \mathbf{0}, \\ & \mathbf{v} \geq \mathbf{0}. \end{aligned} \quad (\text{B.11})$$

where \mathbf{R} is a full column rank matrix satisfying

$$\frac{1}{\beta} \mathbf{P} = \mathbf{R} \mathbf{R}^\top \quad (\text{B.12})$$

(Note that \mathbf{R} may not be a square matrix if \mathbf{P} is not full rank.)

Combining the equivalence between (B.1) and (B.11) and the proposition mentioned in Remark 6, the theorem is proved.

Lemma 12. *For a quadratic programming problem defined by*

$$\begin{aligned} \min_{\mathbf{x}} \quad & \frac{1}{2} \mathbf{x}^\top \mathbf{A} \mathbf{x} + \mathbf{b}^\top \mathbf{x} \\ \text{s.t.} \quad & \mathbf{E} \mathbf{x} = \mathbf{c}, \\ & \mathbf{x} \geq \mathbf{0}. \end{aligned} \quad (\text{B.13})$$

if \mathbf{A} can be decomposed as $\mathbf{A} = \mathbf{R} \mathbf{R}^\top$ with \mathbf{R} being full column rank and there is an optimal solution to (B.13), then the minimum of (B.13) is equal to the maximum of the following problem:

$$\begin{aligned} \max_{\boldsymbol{\alpha}, \mathbf{v}, \boldsymbol{\theta}} \quad & -\frac{1}{2} \boldsymbol{\theta}^\top \boldsymbol{\theta} + \mathbf{c}^\top \boldsymbol{\alpha} \\ \text{s.t.} \quad & \mathbf{b}^\top - \boldsymbol{\alpha}^\top \mathbf{E} - \mathbf{v}^\top = \boldsymbol{\theta}^\top \mathbf{R}^\top, \\ & \mathbf{v} \geq \mathbf{0}. \end{aligned} \quad (\text{B.14})$$

Proof. The Lagrangian of (B.13) is

$$\mathcal{L}(\mathbf{x}, \boldsymbol{\alpha}, \mathbf{v}) = \frac{1}{2} \mathbf{x}^\top \mathbf{A} \mathbf{x} + (\mathbf{b}^\top - \boldsymbol{\alpha}^\top \mathbf{E} - \mathbf{v}^\top) \mathbf{x} + \mathbf{c}^\top \boldsymbol{\alpha} \quad (\text{B.15})$$

Then the dual problem of (B.13) can be written as

$$\begin{aligned} \max_{\boldsymbol{\alpha}, \mathbf{v}} \quad & g(\boldsymbol{\alpha}, \mathbf{v}) \\ \text{s.t.} \quad & \mathbf{v} \geq \mathbf{0}. \end{aligned} \quad (\text{B.16})$$

with

$$g(\boldsymbol{\alpha}, \mathbf{v}) = \inf_{\mathbf{x}} \mathcal{L}(\mathbf{x}, \boldsymbol{\alpha}, \mathbf{v}) \quad (\text{B.17})$$

We now analyze the value of $g(\boldsymbol{\alpha}, \mathbf{v})$ in different cases.

Algorithm 2 Optimization procedure for MMC

- 1: generate a coarse-grained set S^c with cardinality N^c and normalized weights $\mathbf{c} = (c_1, \dots, c_{N^c})^\top$ from \mathcal{S} by the k -medoids algorithm
 - 2: solve the MMC problem on S^c by the SDP relaxation algorithm [40] to get class labels $\mathbf{y}^c = (y_1^c, \dots, y_{N^c}^c)$ of S^c
 - 3: calculate class labels $\mathbf{y}^{(0)} = (y_1, \dots, y_{|\mathcal{S}|})$ of data points in \mathcal{S} from \mathbf{y}^c
 - 4: solve the MMC problem on \mathcal{S} by the local search algorithm proposed in [43] starting from $\mathbf{y} = \mathbf{y}^{(0)}$.
-

Algorithm 3 Optimization procedure for PCCA+

- 1: partition all the data into N^c bins $\mathbf{x}_1^c, \dots, \mathbf{x}_{N^c}^c$ by the k -medoids algorithm
 - 2: estimate the transition matrix $\mathbf{P} = [P_{ij}] = [\Pr(\mathbf{x}_{t+\Delta t} \in \mathbf{x}_j^c | \mathbf{x}_t \in \mathbf{x}_i^c)]$ by the maximum likelihood algorithm in [7]
 - 3: apply the Markov compression algorithm in [26] to lump the N^c bins into κ metastable state.
-

Case (i) There is a $\boldsymbol{\theta}$ such that

$$\mathbf{b}^\top - \boldsymbol{\alpha}^\top \mathbf{E} - \mathbf{v}^\top = \boldsymbol{\theta}^\top \mathbf{R}^\top \quad (\text{B.18})$$

We have $\mathcal{L}(\mathbf{x}, \boldsymbol{\alpha}, \mathbf{v}) = \frac{1}{2} (\mathbf{R}^\top \mathbf{x})^\top (\mathbf{R}^\top \mathbf{x}) + \boldsymbol{\theta}^\top (\mathbf{R}^\top \mathbf{x}) + \mathbf{c}^\top \boldsymbol{\alpha}$ and $g(\boldsymbol{\alpha}, \mathbf{v}) = -\frac{1}{2} \boldsymbol{\theta}^\top \boldsymbol{\theta} + \mathbf{c}^\top \boldsymbol{\alpha}$.

Case (ii) There is no $\boldsymbol{\theta}$ satisfying (B.18). It is easy to see that we can find an \mathbf{x} such that $\mathbf{R}^\top \mathbf{x} = 0$ and $(\mathbf{b}^\top - \boldsymbol{\alpha}^\top \mathbf{E} - \mathbf{v}^\top) \mathbf{x} \neq 0$. Then $g(\boldsymbol{\alpha}, \mathbf{v}) = -\infty$.

Combining the above results yields the conclusion of the lemma. \square

Appendix C. Optimization procedure for MMC

The optimization algorithm for solving MMC problems in our experiments is described by Algorithm 2. It can be seen that this algorithm also combines global search and local search techniques through coarse graining like the algorithm for M³C proposed in this paper.

Appendix D. Implementation procedure of PCCA+

In this paper, we perform the PCCA+ clustering as shown in Algorithm 3.

Appendix E. Description of Model I and Model II

Model I is governed by the Fokker-Planck equation

$$d\mathbf{x}_t = - \begin{bmatrix} \frac{1}{4} \frac{\partial}{\partial x^{(1)}} \\ 9 \frac{\partial}{\partial x^{(2)}} \end{bmatrix} U_I(\mathbf{x}) dt + \begin{bmatrix} \frac{\sqrt{2}}{2} \\ 3\sqrt{2} \end{bmatrix} d\mathbf{u}_t \quad (\text{E.1})$$

where $\mathbf{x}_t = (x_t^{(1)}, x_t^{(2)})$ denotes the system state at time t , \mathbf{u}_t is a two-dimensional Wiener process, and

$$\begin{aligned}
 U_I(\mathbf{x}) = & -8 \sum_{(\mu_1, \mu_2) \in \{-1, 0, 1\} \times \{-\frac{1}{8}, \frac{1}{8}\}} \exp \left(-8 \left(x^{(1)} - \mu_1 \right)^2 \right. \\
 & \left. - 200 \left(\frac{x^{(2)}}{6} - \mu_2 \right)^2 \right) \\
 & + \frac{4}{5} \left(x^{(1)} \right)^4 + \frac{16}{9} \left(x^{(2)} \right)^2
 \end{aligned} \tag{E.2}$$

The stochastic differential equation of Model II is

$$d\mathbf{x}_t = -\frac{1}{\gamma} \begin{bmatrix} \frac{\partial}{\partial x^{(1)}} \\ \frac{\partial}{\partial x^{(2)}} \end{bmatrix} U_{II}(\mathbf{x}) dt + \sqrt{\frac{2}{\gamma}} d\mathbf{u}_t \tag{E.3}$$

with

$$\begin{aligned}
 U_{II}(\mathbf{x}) = & -4\gamma \exp \left(-16 \left((\|\mathbf{x}\| - 1.6)^2 + \max \left\{ \theta - \frac{\pi}{2}, 0 \right\}^2 \right) \right) \\
 & -4\gamma \exp \left(-0.8 \left(x^{(1)} + 1 \right)^2 - 32 \left(x^{(2)} - 0.5 \right)^2 \right) \\
 & -4\gamma \exp \left(-0.8 \left(x^{(1)} + 1 \right)^2 - 32 \left(x^{(2)} + 0.5 \right)^2 \right) \\
 & + \frac{1}{5} \gamma \left(\left(x^{(1)} \right)^4 + \left(x^{(2)} \right)^4 \right)
 \end{aligned} \tag{E.4}$$

$\theta = \text{atan2}(x^{(2)}, x^{(1)})$ and $\gamma = 1.67$. It is easy to verify that Model I and Model II are time-reversible diffusion processes, and their equilibrium distributions are $\pi(\mathbf{x}) \propto \exp(-U_I(\mathbf{x}))$ and $\pi(\mathbf{x}) \propto \exp(-U_{II}(\mathbf{x}))$ separately.

Moreover, we utilize the Euler-Maruyama method [63] to solve (E.1) and (E.2) in this paper.

References

- [1] H. Wu, Maximum margin clustering for state decomposition of metastable systems, in: I. Rojas, G. Joya, J. Cabestany (Eds.), Proceedings of the 12th International Work-Conference on Artificial Neural Networks, Vol. 7902 of Lecture Notes in Computer Science, Springer, Tenerife, Spain, 2013, pp. 556–565.
- [2] F. Noé, S. Fischer, Transition networks for modeling the kinetics of conformational change in macromolecules, *Current opinion in structural biology* 18 (2) (2008) 154–162.
- [3] T. Biancalani, T. Rogers, A. McKane, Noise-induced metastability in biochemical networks, *Physical Review E* 86 (1) (2012) 010106.

- [4] N. Berglund, B. Gentz, Metastability in simple climate models: Pathwise analysis of slowly driven langevin equations, *Stochastics and Dynamics* 2 (03) (2002) 327–356.
- [5] F. Noé, I. Horenko, C. Schütte, J. Smith, Hierarchical analysis of conformational dynamics in biomolecules: Transition networks of metastable states, *Journal of Chemical Physics* 126 (2007) 155102.
- [6] C. R. Schwantes, V. S. Pande, Improvements in markov state model construction reveal many non-native interactions in the folding of ntl9, *Journal of chemical theory and computation* 9 (4) (2013) 2000–2009.
- [7] J. Prinz, H. Wu, M. Sarich, B. Keller, M. Senne, M. Held, J. Chodera, C. Schütte, F. Noé, Markov models of molecular kinetics: Generation and validation, *Journal of Chemical Physics* 134 (2011) 174105.
- [8] R. Aldhaferi, H. Khalil, Aggregation and optimal control of nearly completely decomposable Markov chains, in: *Proceedings of the 28th IEEE Conference on Decision and Control*, IEEE, 1989, pp. 1277–1282.
- [9] J. Chodera, W. Swope, J. Pitnera, K. Dill, Long-time protein folding dynamics from short-time molecular dynamics simulations, *Multiscale Modeling & Simulation* 5 (4) (2006) 1214–1226.
- [10] M. Sarich, F. Noé, C. Schütte, On the approximation quality of Markov state models, *SIAM Multiscale Model. Simul.* 8 (4) (2010) 1154–1177.
- [11] J. D. Chodera, F. Noé, Markov state models of biomolecular conformational dynamics, *Current Opinion in Structural Biology* 25 (2014) 135–144.
- [12] F. Noé, H. Wu, J.-H. Prinz, N. Plattner, Projected and hidden markov models for calculating kinetics and metastable states of complex molecules, *The Journal of chemical physics* 139 (18) (2013) 184114.
- [13] N. Groningen, Essential dynamics of reversible peptide folding: memory-free conformational dynamics governed by internal hydrogen bonds, *Journal of Molecular Biology* 309 (1) (2001) 299–313.
- [14] W. Swope, J. Pitnera, F. Suits, M. Pitman, M. Eleftheriou, B. Fitch, R. Germain, A. Rayshubski, T. Ward, Y. Zhestkov, R. Zhou, Describing protein folding kinetics by molecular dynamics simulations. 2. example applications to alanine dipeptide and a β -hairpin peptide, *Journal of Physical Chemistry B* 108 (21) (2004) 6582–6594.
- [15] E. Sorin, V. Pande, Exploring the helix-coil transition via all-atom equilibrium ensemble simulations, *Biophysical Journal* 88 (4) (2005) 2472–2493.
- [16] S. Elmer, S. Park, V. Pande, Foldamer dynamics expressed via markov state models. II. state space decomposition, *Journal of chemical physics* 123 (2005) 114903.

- [17] O. M. Becker, Geometric versus topological clustering: an insight into conformation mapping, *Proteins: Structure, Function, and Bioinformatics* 27 (2) (1997) 213–226.
- [18] X. Daura, W. F. van Gunsteren, A. E. Mark, Folding–unfolding thermodynamics of a β -heptapeptide from equilibrium simulations, *Proteins: structure, function, and bioinformatics* 34 (3) (1999) 269–280.
- [19] D. Chema, A. Goldblum, The “nearest single neighbor” method finding families of conformations within a sample, *Journal of chemical information and computer sciences* 43 (1) (2003) 208–217.
- [20] A. Glättli, D. Seebach, W. F. van Gunsteren, Do valine side chains have an influence on the folding behavior of β -substituted β -peptides?, *Helvetica chimica acta* 87 (10) (2004) 2487–2506.
- [21] J. Shao, S. W. Tanner, N. Thompson, T. E. Cheatham, Clustering molecular dynamics trajectories: 1. characterizing the performance of different clustering algorithms, *Journal of Chemical Theory and Computation* 3 (6) (2007) 2312–2334.
- [22] Y. Yao, J. Sun, X. Huang, G. R. Bowman, G. Singh, M. Lesnick, L. J. Guibas, V. S. Pande, G. Carlsson, Topological methods for exploring low-density states in biomolecular folding pathways, *Journal of chemical physics* 130 (2009) 144115.
- [23] B. Keller, X. Daura, W. F. van Gunsteren, Comparing geometric and kinetic cluster algorithms for molecular simulation data, *Journal of chemical physics* 132 (7) (2010) 074110.
- [24] F. Noé, C. Schütte, E. Vanden-Eijnden, L. Reich, T. R. Weikl, Constructing the equilibrium ensemble of folding pathways from short off-equilibrium simulations, *Proceedings of the National Academy of Sciences* 106 (45) (2009) 19011–19016.
- [25] P. Deuffhard, W. Huisinga, A. Fischer, C. Schütte, Identification of almost invariant aggregates in reversible nearly uncoupled markov chains, *Linear Algebra and its Applications* 315 (1) (2000) 39–59.
- [26] P. Deuffhard, M. Weber, Robust perron cluster analysis in conformation dynamics, *Linear algebra and its applications* 398 (2005) 161–184.
- [27] V. Mehrmann, D. Szyld, E. Virnik, An SVD approach to identifying metastable states of Markov chains, *Electronic Transactions on Numerical Analysis* 29 (2008) 46–69.
- [28] A. Jain, G. Stock, Identifying metastable states of folding proteins, *Journal of Chemical Theory and Computation* 8 (10).

- [29] G. R. Bowman, Improved coarse-graining of markov state models via explicit consideration of statistical uncertainty, *Journal of chemical physics* 137 (2012) 134111.
- [30] E. H. Kellogg, O. F. Lange, D. Baker, Evaluation and optimization of discrete state models of protein folding, *Journal of Physical Chemistry B* 116 (37) (2012) 11405–11413.
- [31] R. T. McGibbon, C. R. Schwantes, V. S. Pande, Statistical model selection for markov models of biomolecular dynamics, *Journal of Physical Chemistry B*.
- [32] J. Chodera, N. Singhal, V. Pande, K. Dill, W. Swope, Automatic discovery of metastable states for the construction of markov models of macromolecular conformational dynamics, *Journal of Chemical Physics* 126 (2007) 155101.
- [33] K. Crammer, Y. Singer, On the algorithmic implementation of multiclass kernel-based vector machines, *Journal of Machine Learning Research* 2 (2001) 265–292.
- [34] L. Xu, Convex large margin training techniques: Unsupervised, semi-supervised, and robust support vector machines, Ph.D. thesis, University of Waterloo, Waterloo, Ontario, Canada (2007).
- [35] V. Vapnik, *Statistical Learning Theory*, Wiley, New York, 1998.
- [36] L. Bottou, C. Cortes, J. S. Denker, H. Drucker, I. Guyon, L. D. Jackel, Y. LeCun, U. A. Muller, E. Sackinger, P. Simard, V. Vapnik, Comparison of classifier methods: a case study in handwriting digit recognition, in: *Proceedings of the 12th International Conference on Pattern Recognition*, Vol. 2, IEEE, IEEE Computer Society Press, 1994, pp. 77–82.
- [37] J. Friedman, Another approach to polychotomous classification, Tech. rep., Department of Statistics, Stanford University (1996).
- [38] E. L. Allwein, R. E. Schapire, Y. Singer, Reducing multiclass to binary: A unifying approach for margin classifiers, *Journal of Machine Learning Research* 1 (2001) 113–141.
- [39] L. Xu, J. Neufeld, B. Larson, D. Schuurmans, Maximum margin clustering, *Advances in Neural Information Processing Systems* 17 (2004) 1537–1544.
- [40] L. Xu, D. Schuurmans, Unsupervised and semi-supervised multi-class support vector machines, in: *Proceedings of the National Conference on Artificial Intelligence*, Vol. 20, AAAI, 2005, p. 904.
- [41] H. Valizadegan, R. Jin, Generalized maximum margin clustering and unsupervised kernel learning, in: *Advances in Neural Information Processing Systems*, Vol. 19, 2006, pp. 1417–1424.

- [42] B. Zhao, F. Wang, C. Zhang, Efficient multiclass maximum margin clustering, in: Proceedings of the 25th International Conference on Machine learning, ACM, 2008, pp. 1248–1255.
- [43] K. Zhang, I. Tsang, J. Kwok, Maximum margin clustering made practical, IEEE Transactions on Neural Networks 20 (4) (2009) 583–596.
- [44] A. Rahimi, B. Recht, Random features for large-scale kernel machines, in: J. Platt, D. Koller, Y. Singer, S. Roweis (Eds.), Advances in Neural Information Processing Systems, Vol. 20, MIT Press, Cambridge, MA, 2008, pp. 1177–1184.
- [45] N. Pham, R. Pagh, Fast and scalable polynomial kernels via explicit feature maps, in: Proceedings of the 19th ACM SIGKDD International Conference on Knowledge Discovery and Data Mining, ACM, New York, 2013, pp. 239–247.
- [46] N. Kwak, Nonlinear projection trick in kernel methods: An alternative to the kernel trick, IEEE Transactions on Neural Networks and Learning Systems 24 (12) (2013) 2113–2119.
- [47] R. Horn, C. Johnson, Matrix analysis, Cambridge university press, New York, 1988.
- [48] K. Genova, V. Guliashki, Linear integer programming methods and approaches—a survey, Cybernetics And Information Technologies 11 (1).
- [49] MOSEK ApS, Mosek: High performance software for large-scale LP, QP, SOCP, SDP and MIP including interfaces to C, Java, MATLAB, .NET, R and Python, version 7.0, <http://www.mosek.com> (2012).
- [50] Gurobi Optimization Inc., Gurobi optimizer: State-of-the-art mathematical programming solver, version 5.6, <http://www.gurobi.com/> (2014).
- [51] J. Pryor, J. W. Chinneck, Faster integer-feasibility in mixed-integer linear programs by branching to force change, Computers & Operations Research 38 (8) (2011) 1143–1152.
- [52] T. Hastie, R. Tibshirani, J. J. H. Friedman, The elements of statistical learning, Springer, New York, 2001.
- [53] M. Grant, S. Boyd, CVX: Matlab software for disciplined convex programming, version 2.0 beta, <http://cvxr.com/cvx> (2013).
- [54] M. Weber, Improved Perron cluster analysis, Tech. Rep. ZIB-Report 03-04, Konrad-Zuse-Zentrum für Informationstechnik Berlin (2003).
- [55] A. Asuncion, D. Newman, UCI machine learning repository, <http://www.ics.uci.edu/~mllearn/MLRepository.html> (2007).

- [56] F. Nüske, B. G. Keller, A. S. M. Guillermo Pérez-Hernández, F. Noé, Variational approach to molecular kinetics, submitted to *Journal of Chemical Theory and Computation* (2013).
- [57] F. Noé, F. Nüske, A variational approach to modeling slow processes in stochastic dynamical systems, *SIAM Multiscale Model. Simul.* 11 (2) (2013) 635–655.
- [58] S. Shalev-Shwartz, Y. Singer, N. Srebro, A. Cotter, Pegasos: Primal estimated sub-gradient solver for svm, *Mathematical programming* 127 (1) (2011) 3–30.
- [59] I. W. Tsang, J. T. Kwok, P.-M. Cheung, Core vector machines: Fast svm training on very large data sets, in: *Journal of Machine Learning Research*, 2005, pp. 363–392.
- [60] G. Pérez-Hernández, F. Paul, T. Giogino, G. de Fabritiis, F. Noé, Identification of slow molecular order parameters for markov model construction, *Journal of Chemical Physics* 139 (2013) 015102.
- [61] A. Bellet, A. Habrard, M. Sebban, A survey on metric learning for feature vectors and structured data, *CoRR:abs/1306.6709*, <http://arxiv.org/abs/1306.6709> (2013).
- [62] S. Boyd, L. Vandenberghe, *Convex Optimization*, Cambridge University Press, New York, 2004.
- [63] P. E. Kloeden, R. Pearson, *Numerical Solution of Stochastic Differential Equations*, Springer, Berlin, 1992.